Technical and Interpretive Pitfalls in Adrenal Imaging

Gurinder Nandra, MBChB, BSc
Oliver Duxbury, MBBCh, BSc
Pawan Patel, MBBS, BSc
Jaymin H. Patel, MBBS, BSc
Nirav Patel, BSc, MBBS, MRCS
Ioannis Vlahos, BSc, MBBS, MRCP

Abbreviations: ACTH = adrenocorticotropic hormone, FDG = fluorine 18 fluorodeoxyglucose, FIESTA = fast imaging employing steady-state acquisition, PPNAD = primary pigmented nodular adrenal dysplasia, ROI = region of interest

RadioGraphics 2020; 40:1041–1060

https://doi.org/10.1148/rg.2020190080

Content Codes: CT GU MR SQ

From the Department of Radiology, St George's Hospital NHS Trust, Blackshaw Road, London SW17 0QT, England. Recipient of a Cum Laude award for an education exhibit at the 2018 RSNA Annual Meeting. Received March 24, 2019; revision requested September 3 and received October 1; accepted October 16. For this journal-based SA-CME activity, the authors, editor, and reviewers have disclosed no relevant relationships. **Address correspondence to** G.N. (e-mail: *gnandra@doctors.org.uk*).

SA-CME LEARNING OBJECTIVES

After completing this journal-based SA-CME activity, participants will be able to:

- Identify and avoid technical pitfalls encountered at adrenal imaging.
- Describe and avoid interpretive pitfalls, including mimics of adrenal pathologic conditions.
- Recognize imaging features that may suggest an endocrine disturbance or specific endocrine conditions.

See rsna.org/learning-center-rg.

The adrenal gland may exhibit a wide variety of pathologic conditions. A number of imaging techniques can be used to characterize these, although it is not always possible to attain a definitive diagnosis radiologically. Incorrect diagnoses may be made if radiologists are not attentive to technical parameters and interpretive factors associated with adrenal gland imaging. Hence, an appreciation of the intricacies of adrenal imaging strategies and characterization is required; this can be aided by understanding the pitfalls of adrenal imaging. Technical pitfalls at CT may relate to the imaging parameters, including region of interest characteristics, tube voltage selection, and the timing of contrast material–enhanced imaging. With MRI, imaging acquisition technique and evaluation of the reference tissues used in chemical shift MRI are important considerations that can directly influence image interpretation. Interpretive errors may occur when evaluating adrenal washout at CT without considering other radiologic features, including the size of adrenal nodules, the presence of fat or calcification, the attenuation of nodules, and atypical imaging features. The characterization of an incidental adrenal lesion as benign or malignant does not end the role of the radiologist; consideration as to whether an adrenal lesion is associated with endocrine dysfunction is required. While imaging may not be optimal for establishing endocrine activity, there are imaging features from which radiologists may infer function. In cases of known endocrine activity, imaging can guide clinical management, including further investigations such as venous sampling.

Introduction

Incidental adrenal masses larger than 1 cm in size are common findings, identified in approximately 5% of patients undergoing CT, with an increasing prevalence with age (1,2). While these lesions may require radiologic workup, most ultimately prove to be benign and do not result in a clinically significant endocrine disturbance. Benign adenomas are statistically the most common adrenal pathologic condition encountered at imaging. The probability of encountering malignant adrenal lesions is low, although the risk clearly increases in patients with a known malignancy elsewhere (3,4).

While imaging can be useful for the characterization of adrenal lesions, particularly adenomas, it is not always possible to attain a definitive diagnosis radiologically. Moreover, the low prevalence of clinically significant and nonadenomatous pathologic conditions may mean radiologists are not as familiar with the radiologic characteristics of such pathologic conditions or the appropriate imaging strategies used to investigate them. Erroneous diagnoses may be reached if the technical and interpretive factors associated with the relevant imaging strategies are not closely considered. An understanding of the pitfalls of adrenal imaging is imperative to improve the accuracy

TEACHING POINTS

- Chemical shift MRI and nonenhanced CT help identify the same property of an adrenal nodule, namely the presence of microscopic fat content. Therefore, in general terms, if a lesion does not demonstrate microscopic fat at CT (attenuation >10 HU), it is unlikely to satisfy criteria for intracytoplasmic fat at chemical shift MRI. In practice, studies have shown that chemical shift MRI is sensitive in identifying adenomas in nodules identified at nonenhanced CT that are less than 20 HU. A potential imaging strategy pitfall would be to assess nodules with even greater attenuation values (>20–30 HU) with chemical shift MRI when evaluation of enhancement kinetics with CT is more likely to be additive.
- The shortest echo time should be used to negate the effect that T2* decay has in reducing measured T1 signal intensity, which can be misinterpreted on the out-of-phase images as signal loss. The out-of-phase echo image should be acquired before the in-phase echo image to minimize T2* decay on the out-of-phase echo image.
- Analysis of adrenal masses solely based on washout values can be misleading, as other criteria such as the size of a lesion, peak enhancement values, and lesion heterogeneity should equally be considered.
- The anatomy and pathologic conditions arising adjacent to the adrenal gland can simulate adrenal lesions.
- While CT or MRI cannot consistently help determine endocrine dysfunction, certain radiologic features may manifest that suggest altered endocrine function. If the patient is already known to have endocrine dysfunction, radiologic interpretation should include additional considerations.

of image interpretation and to provide radiologists with an appreciation of the intricacies of adrenal imaging strategies.

This article highlights the potential pitfalls encountered at adrenal imaging, mainly related to CT and MRI. These include technical pitfalls, interpretive errors including mimics of adrenal pathologic conditions, and imaging features that may suggest endocrine disturbance or specific endocrine conditions.

Technical Pitfalls: CT

Region of Interest Characteristics

The size of a region of interest (ROI) can influence the reported attenuation value of an adrenal nodule. The initial studies that established non–contrast material–enhanced attenuation criteria for lipid-rich adenomas and parameters for washout typically used an ROI covering two-thirds of the lesion (5–7). The use of a smaller ROI to selectively identify isolated regions of microscopic lipid (≤10 HU) risks sampling areas of lesional variation or image noise, resulting in an erroneous representation of the entire lesion (Fig 1) (8,9). When selecting an ROI, the periphery of an adrenal nodule should be excluded to negate partial volume averaging of the adjacent retroperitoneal fat. A technique to ensure that an ROI extending toward the periphery of an adrenal nodule does not cause partial volume effect in the adjacent fat in the z-axis is to ensure the ROI would remain within the lesion on the sections above and below the section selected to measure the ROI. It is recommended that an ROI should be measured on images with 3-mm collimation, a value that balances the trade-off between spatial resolution and image noise (10). Small areas of heterogeneity (eg, flecks of calcification or areas of necrosis) are unlikely to be representative of the adrenal pathologic condition and should also be excluded from measurements (9).

Attenuation Values at Nonenhanced CT

Adenomas are by far the most prevalent adrenal tumor and the commonest radiologic diagnosis for incidental adrenal lesions. A nonenhanced CT attenuation value less than or equal to 10 HU can be used to diagnose lipid-rich adrenal adenomas (sensitivity 71%, specificity 98%) (11). An adrenal nodule identified at nonenhanced CT with an attenuation value greater than 10 HU cannot be confirmed as an adenoma without further imaging, which could include washout CT and potentially chemical shift MRI.

Chemical shift MRI and nonenhanced CT help identify the same property of an adrenal nodule, namely the presence of microscopic fat content. Therefore, in general terms, if a lesion does not demonstrate microscopic fat at CT (attenuation >10 HU), it is unlikely to satisfy criteria for intracytoplasmic fat at chemical shift MRI. In practice, studies have shown that chemical shift MRI is sensitive in identifying adenomas in nodules identified at nonenhanced CT that are less than 20 HU. A potential imaging strategy pitfall would be to assess nodules with even greater attenuation values (>20–30 HU) with chemical shift MRI when evaluation of enhancement kinetics with CT is more likely to be additive (Fig 2). The sensitivity of adrenal washout CT in identifying adenomas with a nonenhanced attenuation greater than 20 HU has been reported to be as high as 100% in select studies, in comparison to that of 64% with chemical shift MRI (12,13).

A potential exception to this guidance may apply when a nodule exceeds 43 HU at nonenhanced CT. If such a nodule is nonhemorrhagic and noncalcified, some limited data suggest that it should be treated as suspicious for malignancy (14). In these cases, fluorine 18 fluorodeoxyglucose (FDG) PET/CT or other cancer-detecting strategies may be considered as the next imaging investigation rather than washout CT or chemical shift MRI (Fig 3).

Figure 1. Altering the size of the ROI. **(a, b)** Axial nonenhanced CT images show an incidental left adrenal nodule. A small ROI measures the attenuation as 19 HU **(a)**. Using an ROI of this size may result in further imaging being performed to characterize the lesion. A larger more appropriately sized ROI covers at least two-thirds of the circumference of the lesion, with an attenuation of 8 HU **(b)**. With a larger ROI, the lesion can be diagnosed as a lipid-rich adenoma without further imaging. Solid circle = ROI, *cm^2* = cm^2, *sd* = standard deviation. Keys are the same for Figures 3–8, 10, 11, and 23.

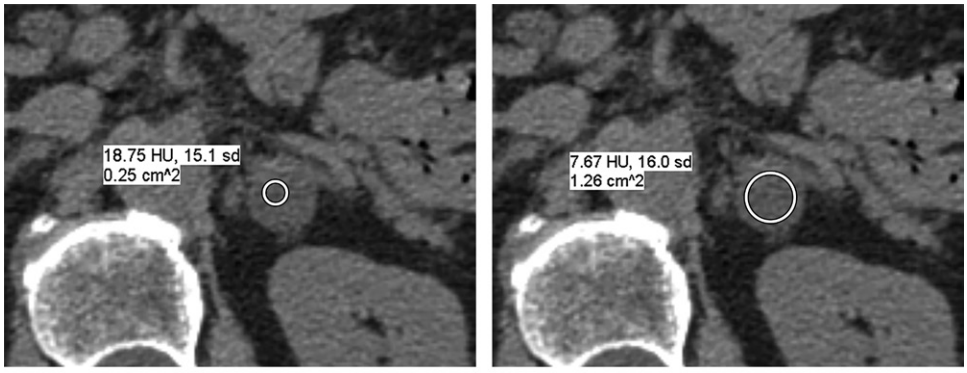

a. **b.**

Figure 2. Evaluation of hyperattenuating nodules at nonenhanced CT. **(a)** Axial nonenhanced CT image shows an indeterminate right adrenal lesion (arrow), with a nonenhanced attenuation of 33 HU, suggesting a lipid-poor adrenal lesion. The patient erroneously underwent chemical shift MRI for further characterization. **(b, c)** Axial in-phase **(b)** and out-of-phase **(c)** chemical shift MR images show no signal loss, confirming the lesion (arrow) was not a lipid-rich adenoma. The lesion was indeterminate, and additional imaging with chemical shift MRI had not narrowed the differential diagnosis. Homogeneously attenuating lesions greater than 20–30 HU are unlikely to show lipid content at chemical shift MRI. Evaluation of enhancement kinetics with CT washout is more likely to help identify lipid-poor adrenal adenomas and is therefore preferable to chemical shift MRI.

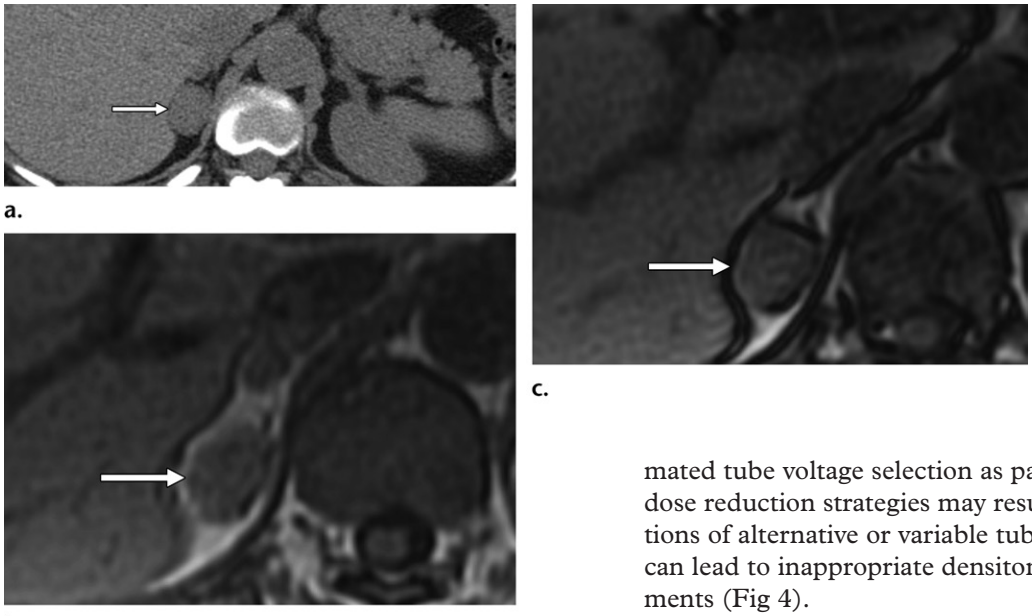

a. **c.**

b.

Effect of Tube Voltage on Attenuation Values

Altering the tube voltage influences densitometry measurements of all soft tissues, including the adrenal glands (15). Therefore, it is important to use an appropriate tube voltage when performing nonenhanced adrenal CT and CT washout examinations. The majority of the studies regarding CT adrenal gland characterization used a tube voltage of 120 kVp (10,16). The advent of automated tube voltage selection as part of automatic dose reduction strategies may result in acquisitions of alternative or variable tube voltage, which can lead to inappropriate densitometry measurements (Fig 4).

Conversely, imaging at differing tube voltages is an intrinsic part of dual-energy or spectral imaging and can be potentially used to characterize lipid-containing adrenal adenomas. Unlike other soft tissues, lipid characteristically reduces in attenuation on lower kilovolt peak acquisitions (17). Limited studies of incidentally detected adrenal lesions at dual-energy CT suggest that lipid-rich adenomas can be diagnosed by assessing for a reduction in attenuation on lower kilovolt peak acquisitions, with a high specificity (100%) but low sensitivity (50%) (18,19). More studies are required to establish

Figure 3. Evaluation of hyperattenuating nodules at nonenhanced CT. **(a)** Axial nonenhanced CT image in a patient with a history of lung malignancy shows a right adrenal nodule with an attenuation of 45 HU. This was indeterminate based on morphology and washout values at subsequent adrenal washout CT (not shown). **(b)** Axial FDG PET/CT image shows avid uptake (arrow), a finding consistent with metastasis. The hyperattenuating adrenal nodule (>43 HU) at nonenhanced CT raised suspicion for malignancy. FDG PET/CT can be of use in such instances rather than performing further dedicated CT or MRI of the adrenal glands, particularly when there is a known history of malignancy.

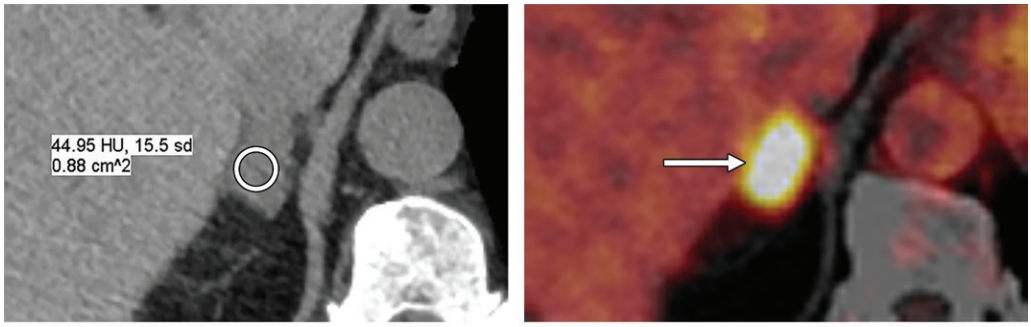

a. b.

Figure 4. **(a–c)** Axial precontrast **(a)**, portal venous phase **(b)**, and 15-minute delayed phase **(c)** adrenal washout CT images obtained by using an erroneous tube voltage show an indeterminate left adrenal nodule (absolute washout = 43%, relative washout = 33%, with > 60% absolute or >40% relative washout being suggestive of an adenoma). Owing to the automatic tube voltage selection, the tube voltage used was 100 kVp, which produced inappropriate measurements of attenuation on the washout examination. These studies should be performed at 120 kVp. **(d, e)** Axial in-phase **(d)** and out-of-phase **(e)** chemical shift MR images show loss of signal within the adrenal lesion, with an adrenal-to-spleen signal intensity ratio of 0.68 (<0.71 indicative of a lipid-rich adenoma), confirming a lipid-rich adenoma. Red dashed circle = ROI selected on the adrenal lesion, blue dashed circle = ROI selected on the spleen.

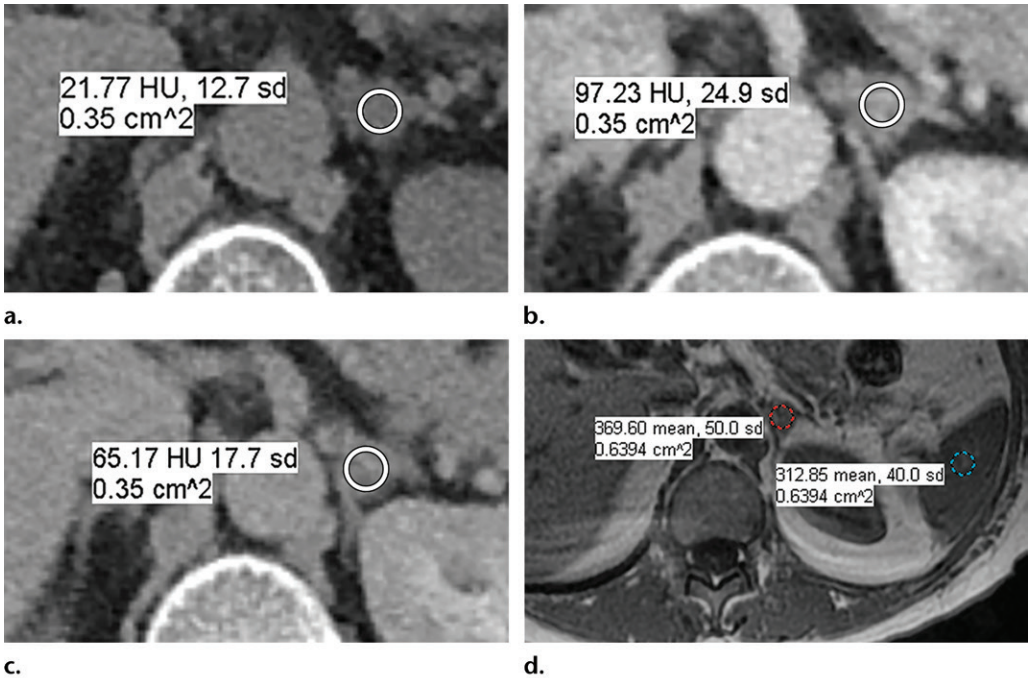

a. b. c. d. e.

values for attenuation change between differing dual-energy or spectral tube voltage combinations (Fig 5).

Contrast-enhanced dual-energy or spectral imaging acquisitions can undergo material differentiation techniques that render virtual noncontrast-enhanced images. Similar to conventional nonenhanced adrenal CT, a cutoff of less than or equal to 10 HU can be used on virtual nonen-

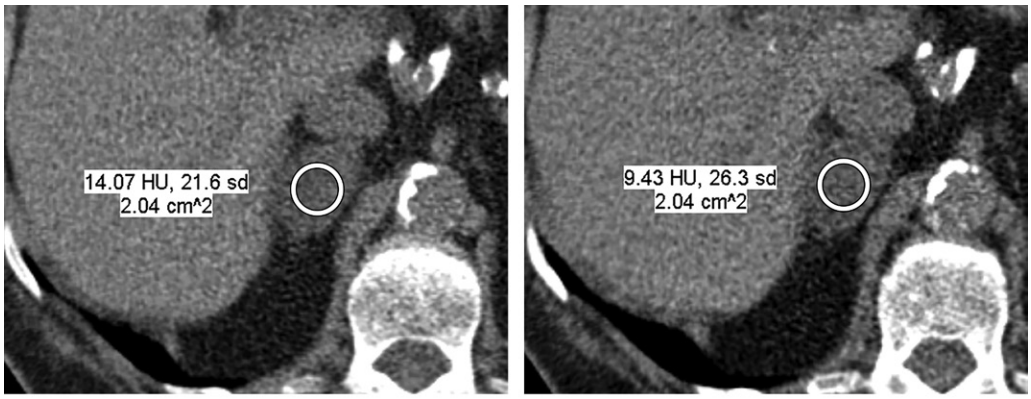

a. b.

Figure 5. Attenuation values at differing tube voltages. Axial nonenhanced dual-energy CT images show a right adrenal nodule with an attenuation of 14 HU at 140 kVp (tin filtered) **(a)** and 9 HU at 100 kVp **(b)**. These attenuation values are contradictory for diagnosing a lipid-rich adenoma (a nonenhanced CT attenuation ≤10 HU is used to diagnose lipid-rich adenomas). However, the reduction of attenuation values on lower kilovolt peak images suggests the presence of lipid content. A diagnosis of a lipid-rich adrenal adenoma can be inferred from the data without the need for further imaging.

hanced images to identify lipid-rich adenomas, with a metaanalysis demonstrating a similar sensitivity in identifying adenomas to conventional nonenhanced images (20).

However, it is important to ensure that such reconstructions are artifact free. In particular, the evaluation of lower kilovolt peak images may be limited by beam hardening and photon starvation effects, which lead to increased image noise and therefore a potential greater variance in reported attenuation values. In addition, there are limited accounts of virtual monoenergetic images being associated with increased noise owing to the extremes of high and low kilovolt peak imaging (21).

Timing of Postcontrast Acquisitions

Following the administration of intravenous contrast material (postcontrast), adenomas typically enhance rapidly and demonstrate rapid washout. Nonadenomatous pathologic conditions including metastases typically enhance rapidly. However, unlike adenomas, they demonstrate a prolonged washout. The observation that adenomatous nodules washout earlier than do nonadenomatous nodules is used in CT washout examinations (22).

Calculations of washout are based on densitometry measurements on delayed postcontrast images relative to the enhancement at portal venous imaging (portal venous phase minus nonenhanced imaging) for absolute washout or portal venous phase attenuation alone for relative washout calculations. An absolute washout value greater than or equal to 60% or a relative washout value greater than or equal to 40% is used to identify adrenal adenomas. For lesions that are indeterminate for lipid-rich adrenal adenomas at nonenhanced CT (ie, attenuation >10 HU), washout examinations can provide a high level of sensitivity and specificity in identifying lipid-poor adenomas. If images obtained before the administration of contrast material (precontrast) are available, calculation of absolute washout is preferable, as studies have demonstrated a greater sensitivity in the detection of adenomas compared with relative washout (86% and 82%, respectively), although specificity is equivalent (92%) (10).

When performing CT adrenal washout examinations, it is recommended that postcontrast images are obtained at 60–90 seconds and 15 minutes (16,23). There is an understandable appeal to using an earlier delayed postcontrast acquisition to shorten the duration of the examination, such as at 10 minutes. However, this may be at the expense of reduced sensitivity, as a proportion of adenomas require a longer period to satisfy the established 15-minute criteria for washout (Fig 6) (24).

Several examinations that are not intended as CT washout examinations may incorporate a postcontrast acquisition at 60–90 seconds and a more delayed acquisition, which is earlier than 15 minutes (Fig 7). These examinations may detect incidental adrenal lesions that can be characterized with such examination protocols, acting as a facsimile of a CT washout examination. Dependent on local protocol, examples of such examinations may include multiphase CT renal-urographic examinations and dual-position contrast-enhanced CT colonography examinations.

If an incidental adrenal lesion satisfies the criteria for washout at delayed phase imaging (although this is earlier than 15 minutes) and there are no other atypical features, an adenoma can be diagnosed without further imaging. If washout criteria have not been satisfied, an adenoma cannot be

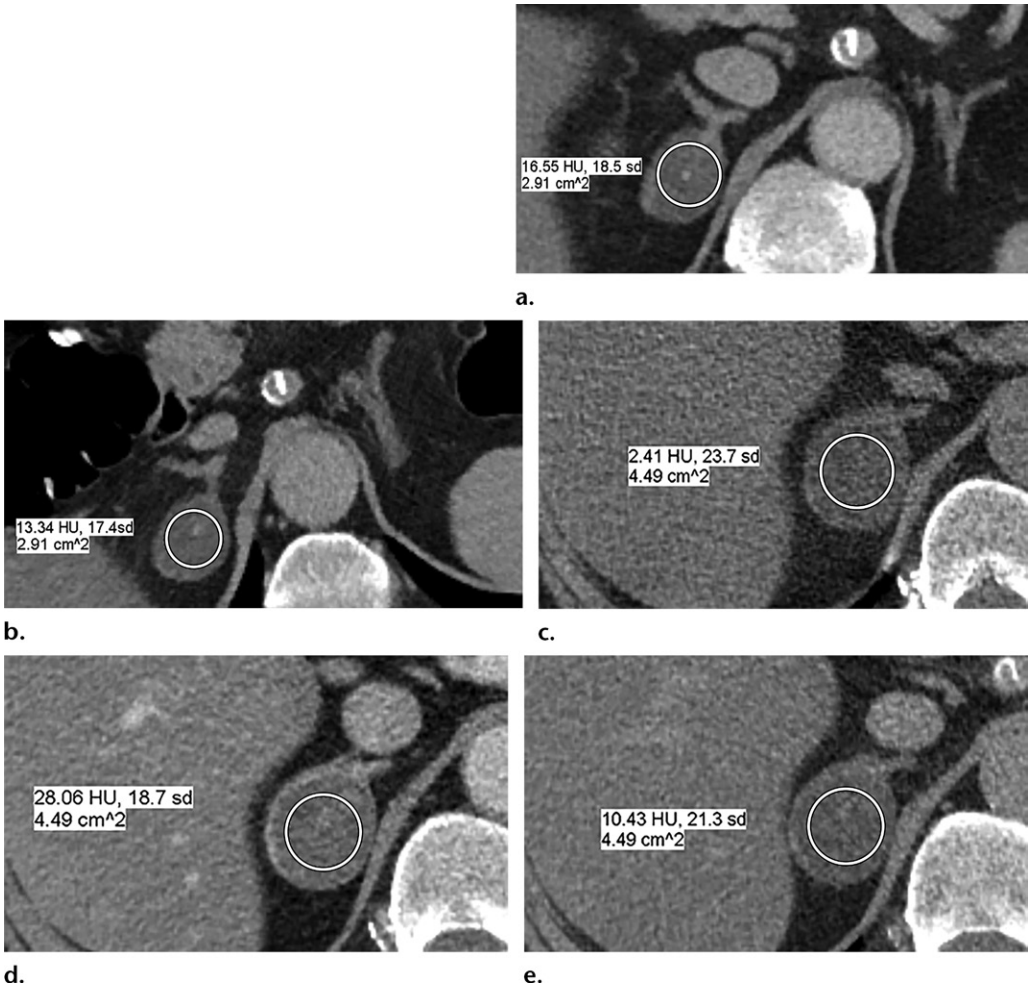

Figure 6. Altering delayed postcontrast imaging timing. **(a, b)** Axial contrast-enhanced CT colonography images obtained in the portal venous phase with the patient in the supine position **(a)** and approximately 3 minutes postcontrast with the patient in the prone position **(b)** show an incidental right adrenal lesion. The lesion remained indeterminate on the basis of the relative washout value on these images (19%), utilizing a prone delayed postcontrast acquisition, in this case obtained at 3 minutes. **(c–e)** Axial precontrast **(c)**, portal venous phase **(d)**, and delayed phase **(e)** images from the CT washout examination show the nodule with a relative washout value of 62.8% (absolute washout, 68.7%), resulting in the diagnosis of an adenoma. A proportion of adenomas take up to 15 minutes to demonstrate sufficient washout to satisfy the established washout cutoffs. In this case, the washout examination could have been terminated after the precontrast acquisition, if the examination had been monitored.

confirmed, and a formal washout study to include a 15-minute acquisition may be needed. Although modified washout thresholds have been suggested for earlier delayed postcontrast acquisitions, this may be at the expense of sensitivity and specificity (24). Careful evaluation of additional series at nondedicated imaging may, therefore, avoid the pitfall of requesting further imaging for adrenal characterization.

Technical Pitfalls: MRI

Reference Tissue

It is generally agreed that qualitative visual assessment and quantitative methods are similar in efficacy for identifying adrenal lesion signal loss at chemical shift MRI (25). Qualitative methods require visual assessment of signal intensity change, usually against a reference tissue, such as the spleen. This may be assisted with the generation of subtraction images to highlight areas of signal loss. Quantitative evaluation includes calculation of signal intensity indices that reflect the percentage of signal loss on out-of-phase images (>16.5% indicates lipid-rich adenomas). Adrenal-to-spleen signal intensity ratios are considered more specific and reflect the ratio of signal loss remaining on out-of-phase images, correcting for splenic signal change (<0.71 indicative of lipid-rich adenomas) (26–28). It should be borne in mind that these values are established from examinations performed by using 1.5-T MR imagers. Alternative parameters exist for 3-T scanners, although these are not as widely used (26).

The spleen is not affected by fatty infiltration and therefore is the usual reference organ when

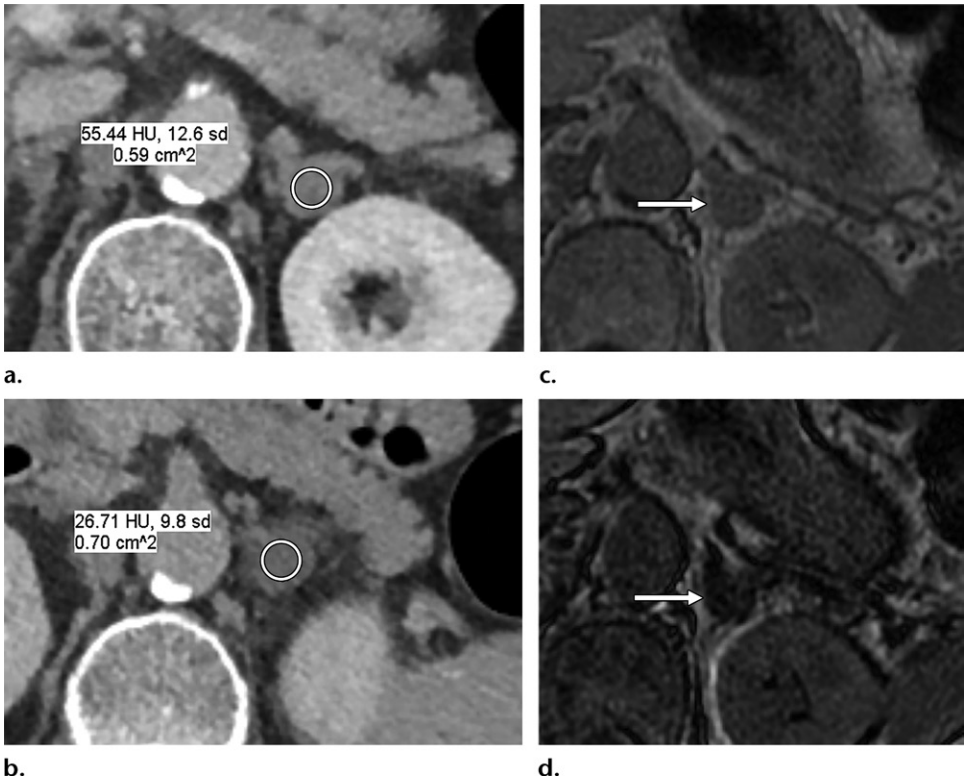

Figure 7. Assessment of washout at nondedicated imaging. **(a, b)** Axial contrast-enhanced CT colonography images obtained in the portal venous phase with the patient in the supine position **(a)** and at 3 minutes postcontrast with the patient in the prone position **(b)** show an incidental left adrenal nodule, which was considered indeterminate. **(c, d)** Axial in-phase **(c)** and out-of-phase **(d)** chemical shift MR images show signal loss within the lesion, consistent with a lipid-rich adenoma (arrow). This diagnosis could have been made at initial imaging without proceeding to further imaging. Relative washout could have been calculated at the nondedicated examination because, in addition to the portal venous phase examination, a delayed postcontrast acquisition had been obtained within 15 minutes. In this case, the relative washout value was 52%. If the washout value did not satisfy the established washout parameters, an adenoma could not have been excluded without further dedicated adrenal imaging.

both qualitatively and quantitatively evaluating for relative signal intensity loss at chemical shift MRI (29). The signal intensity of the spleen should remain consistent at chemical shift MRI, with small variations attributable to technical differences in acquisition of the echo pair. Radiologists must be aware that this premise of splenic signal intensity consistency may be lost, for example in those patients prone to hemosiderin deposition, which can cause elevation of T1 signal intensity at out-of-phase imaging.

Despite this, the spleen is usually still preferred over other organs, such as the liver, as a reference organ, as the hepatic parenchyma can be affected by both fat and hemosiderin deposition. A shortcoming of the alternative use of paraspinal muscles as a reference standard is the varying amounts of interspersed fat identified within these muscles (30).

Technical Parameters

Other technical considerations in chemical shift MRI include performing a single breath-hold dual-echo acquisition rather than two separate breath-hold acquisitions to obtain the echo pair. This is to reduce misregistration and maintain the quality of subtraction analyses (31).

The shortest echo time should be used to negate the effect that T2* decay has in reducing measured T1 signal intensity, which can be misinterpreted on out-of-phase images as signal loss. The out-of-phase echo image should be acquired before the in-phase echo image to minimize T2* decay on the out-of-phase echo image (32).

The in-phase and out-of-phase echo times differ between 1.5-T and 3-T MR imagers. For example, the optimal echo times for a 1.5-T imager may be 2.2 msec (out-of-phase) and 4.4 msec (in-phase) and for a 3-T MR imager may be 1.1 msec and 2.2 msec. Given the short interval and early echo times, it may be technically difficult to acquire the first echo pair with 3-T MR imagers while maintaining image quality. In such cases, the first out-of-phase echo (eg, 1.1 msec) and the second in-phase echo (eg, 4.4 msec) can be used or, alternatively, a Dixon technique can be employed. Deviating from the timings has more significant repercussions at 3-T chemical shift

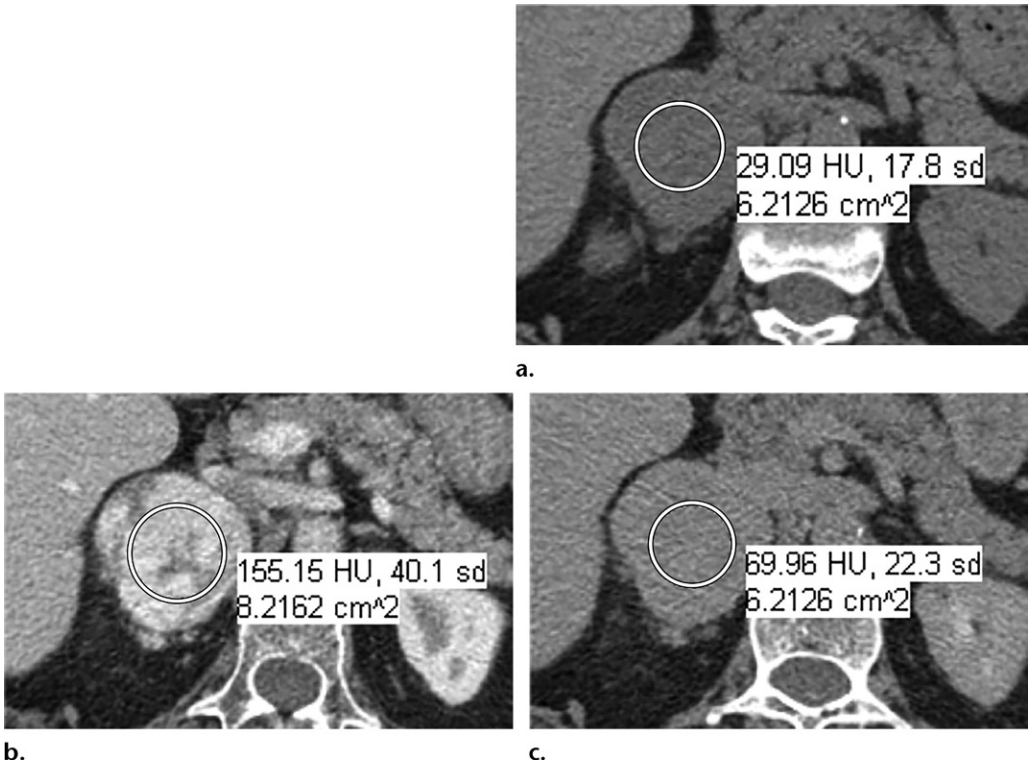

Figure 8. Evaluation of adrenal washout CT. Axial precontrast **(a)**, portal venous phase **(b)**, and 15-minute delayed phase **(c)** CT images show a right adrenal lesion with an absolute washout of 68%, which satisfies the numerical washout criteria for an adenoma. However, the evaluation of CT adrenal washout should also include the evaluation of characteristics other than the washout calculation. The imaging features that suggest that this is not a benign adenoma include the size (>4 cm), heterogeneity of enhancement, and peak enhancement value (>110 HU). The results of histologic evaluation confirmed malignant pheochromocytoma. A peak enhancement greater than 110 HU is classically demonstrated with pheochromocytomas but also with hypervascular metastases. Pheochromocytomas generally demonstrate slow washout but on occasion can exhibit rapid washout, mimicking that of an adenoma.

MRI owing to the shorter interval and earlier echo times (33,34).

Pitfalls in Interpretation

Evaluation of Washout

Analysis of adrenal masses solely based on washout values can be misleading, as other criteria such as the size of a lesion, peak enhancement values, and lesion heterogeneity should equally be considered.

An example of this is pheochromocytoma, which generally demonstrates a slower washout that does not satisfy the washout criteria for an adenoma, although a minority of cases may demonstrate rapid washout, mimicking that of an adenoma (Fig 8). Many of the pheochromocytomas that demonstrate washout within the adenoma range can be differentiated from adenomas by having a high peak enhancement, greater than 110 HU (35). Furthermore, owing to the presence of intracytoplasmic fat and cystic change, the nonenhanced attenuation of pheochromocytomas may occasionally overlap with that of lipid-rich adenomas (36,37). A potential discriminating factor in such instances is the heterogeneity in nonenhanced attenuation that is commonly visualized with pheochromocytomas (35).

Hypervascular metastases, such as those from renal cell carcinoma and hepatocellular carcinoma, are known to demonstrate washout that can satisfy criteria for an adenoma. Therefore, care must be taken in patients with a known primary hypervascular tumor, with consideration of further imaging such as FDG PET/CT, close follow-up, or tissue confirmation (38).

Adrenal Mass Size

Given the relative frequency of encountering small adrenal nodules, studies evaluating adrenal washout CT have been primarily performed with small indeterminate adrenal lesions, with a mean representative adrenal lesion size in some studies of 2.9 cm (11,39). The pretest probability of malignancy significantly increases above 4 cm. Although the precise risk is disputed, figures as high as 70% have been reported for malignancy in lesions greater than 4 cm in size, following the exclusion of myelolipomas and pheochromocytomas (9,40,41).

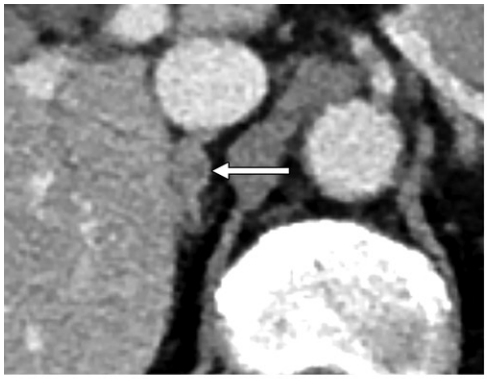

Figure 9. Evaluation of small adrenal nodules. **(a)** Axial CT image shows a minor (7 mm) nodule of the right adrenal gland. Evaluation of the attenuation of this abnormality (arrow) is limited by the partial volume averaging of the adjacent retroperitoneal fat and liver. **(b, c)** Axial in-phase **(b)** and out-of-phase **(c)** MR images are limited by india ink artifact on the out-of-phase sequence, which results in an impression of signal loss (arrow). Per American College of Radiology guidance, adrenal nodules smaller than 1 cm do not generally necessitate further radiologic investigation (16).

a.

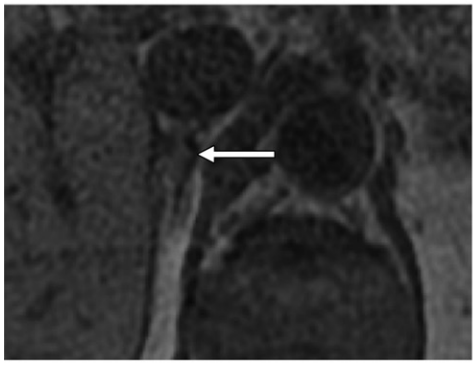

b.

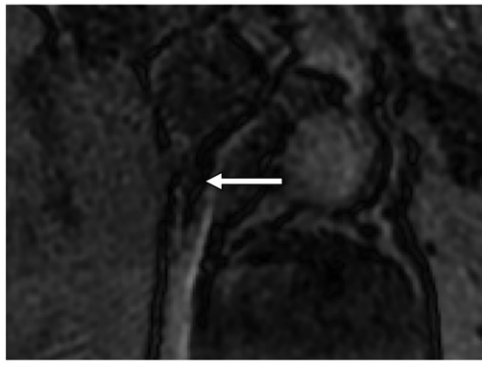

c.

The value of adrenal washout CT and chemical shift MRI in patients with large adrenal masses is far less validated and may be subject to erroneous interpretation. Indeed, as the pretest probability of malignancy is increased, a lesion greater than 4 cm in size is typically recommended for surgical resection, particularly if it cannot be confirmed as being benign and there is no history of primary malignancy elsewhere (16,42). In this clinical scenario, surgery is frequently performed without the need for biopsy. The utilization of a 4-cm cutoff for adrenalectomy demonstrates good sensitivity (93%) in identifying malignancy, although the specificity is low (42%) (43).

At the other end of the spectrum, small lesions pose an imaging dilemma. A potential error is to pursue further radiologic investigation for a minor nodularity that is less than 1 cm in the short axis diameter. The characterization of nodules of this size is often unsuccessful. Therefore, in accordance with American College of Radiology guidance, in general these nodules do not need to be pursued (16). Follow-up may be of use to assess for stability, and an endocrinologic assessment may be considered to determine function in such nodules (42,44).

The evaluation of small nodules is limited at both MRI and CT. India ink artifact can be visualized on out-of-phase gradient-echo sequences at fat-water interfaces. This is due to the admixture of fat and water within the same voxel, which leads to a boundary artifact. When evaluating small nodules at chemical shift MRI, this artifact may give the impression of signal loss and lead to an incorrect diagnosis of a lipid-rich adenoma (Fig 9) (45).

Similarly, CT evaluation of subcentimeter adrenal nodules can be subject to interpretive errors, being limited by partial volume averaging of surrounding retroperitoneal fat, which may lead to erroneously low attenuation values.

Postcontrast Attenuation of Lesions

There are only limited studies suggesting a diagnostic threshold for adenomas at single-phase postcontrast imaging. For example, a threshold less than 18 HU has been observed in one study to diagnose adenomas with high specificity (100%), albeit with low sensitivity (10%) (5). These thresholds have not been successfully validated in larger series across a broad mixture of tumor types. Although intuitively one could assume that in a single postcontrast acquisition a lesion with slightly greater than 10 HU would represent a lipid-rich adenoma that has minimally enhanced, this is counterintuitive to the known physiology of the vast proportion of lipid-poor adenomas, which are expected to enhance rapidly and therefore have higher postcontrast attenuation values. Metastases may also demonstrate rapid enhancement and therefore frequently overlap with adenomas in densitometry measurements at postcontrast imaging (5,46). Therefore, the only pragmatic threshold in single-phase postcontrast imaging is less than

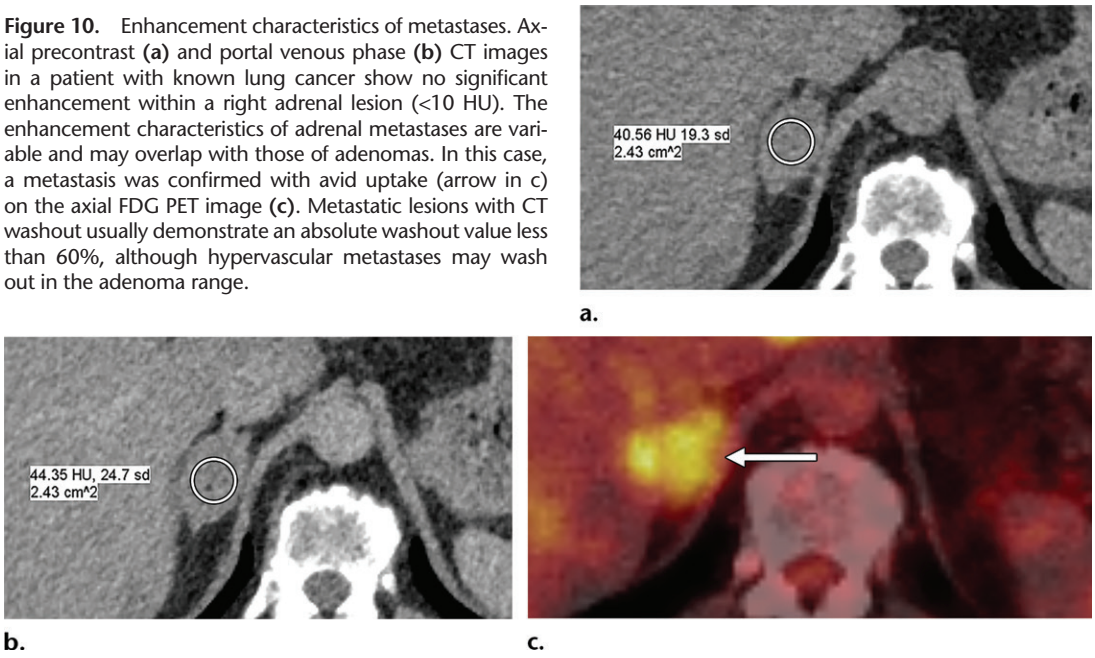

Figure 10. Enhancement characteristics of metastases. Axial precontrast **(a)** and portal venous phase **(b)** CT images in a patient with known lung cancer show no significant enhancement within a right adrenal lesion (<10 HU). The enhancement characteristics of adrenal metastases are variable and may overlap with those of adenomas. In this case, a metastasis was confirmed with avid uptake (arrow in c) on the axial FDG PET image **(c)**. Metastatic lesions with CT washout usually demonstrate an absolute washout value less than 60%, although hypervascular metastases may wash out in the adenoma range.

or equal to 10 HU, as used at nonenhanced CT, accepting that this will have a limited sensitivity for adenoma detection (38,39).

The choices for a lesion measuring greater than 10 HU in a single-phase postcontrast acquisition would include recalling the patient for noncontrast CT or chemical shift MRI or, if the lesion is detected at the time of the examination, performing a delayed acquisition at 15 minutes to calculate relative washout. Notably, in cases in which metastases are a strong clinical concern, FDG PET/CT may be of use (Fig 10), as it has both excellent sensitivity and specificity (97% and 91%, respectively) (47).

Adenomas versus Adrenal Cysts

The attenuation of a lipid-rich adenoma is a reflection of the admixture of soft tissue and intracellular lipid within the lesion, resulting in densitometry measurements that overlap with those of simple cystic lesions. Adrenal cysts are infrequent abnormalities of the adrenal gland that can be misinterpreted as adenomas. Adrenal cysts typically have low attenuation at precontrast imaging but may demonstrate a minor increase at postcontrast imaging owing to pseudoenhancement, akin to that depicted in renal cysts. This is due to factors including beam hardening and partial volume averaging of adjacent enhancing structures (48). In this context, *beam hardening* refers to an observed artifactual increase in reported attenuation values that occurs secondary to the preferential filtration of lower-energy x-ray beams of a polyenergetic x-ray beam as it passes through adjacent structures (49).

This pseudoenhancement is less conspicuous when the enhancement of adjacent structures is reduced in delayed phases. Hence, the reduced pseudoenhancement at delayed phase postcontrast imaging can be misinterpreted as rapid washout, leading to an incorrect diagnosis of an adenoma (Fig 11). An adrenal cyst should be a consideration in cases of adrenal lesions with low attenuation (0–20 HU) that demonstrate low-level enhancement at CT washout. If confirmation is required, MRI may be additive to demonstrate fluid within the cyst.

Adrenal Tumor versus Hematoma

Adrenal hemorrhage should be considered for nonenhancing hyperattenuating (40–60 HU) adrenal lesions, particularly in an appropriate clinical context, such as trauma, bleeding diatheses, and physiologic stress.

It may be challenging to differentiate hemorrhage from other incidentally identified adrenal pathologic conditions. In such cases, assessment of temporal change and evaluation of the periadrenal fat is of use. Periadrenal infiltration or haziness may be visualized from the extension of hematoma into the surrounding tissues (Fig 12) (50). Temporal resolution with a reduction in attenuation is commonly depicted with adrenal hemorrhage at follow-up imaging. Calcification and pseudocyst formation can also occur in the longer term.

A minority of adrenal hemorrhages will occur secondary to an underlying benign or malignant adrenal tumor (eg, myelolipomas, adenomas, pheochromocytomas, and adrenocortical carcinomas) (51,52). Incomplete resolution or an

Figure 11. "Pseudo-washout" in adrenal cysts. **(a–c)** Axial precontrast **(a)**, portal venous phase **(b)**, and 15-minute delayed phase **(c)** CT adrenal washout images show a right adrenal lesion, which may be misinterpreted as an adenoma based on washout calculations (absolute washout value, 77%). Beam-hardening artifact is greatest at initial postcontrast imaging, which artificially increases attenuation values. This pseudoenhancement is less conspicuous when the enhancement of adjacent structures is reduced in the delayed phase. This can lead to the misinterpretation of rapid washout and an incorrect diagnosis of an adenoma. **(d)** Coronal fast imaging employing steady-state acquisition (FIESTA) MR image shows a hyperintense lesion, suggestive of a cyst (arrow). An adrenal cyst should be considered in adrenal lesions with low attenuation (0–20 HU) that demonstrate low-level enhancement.

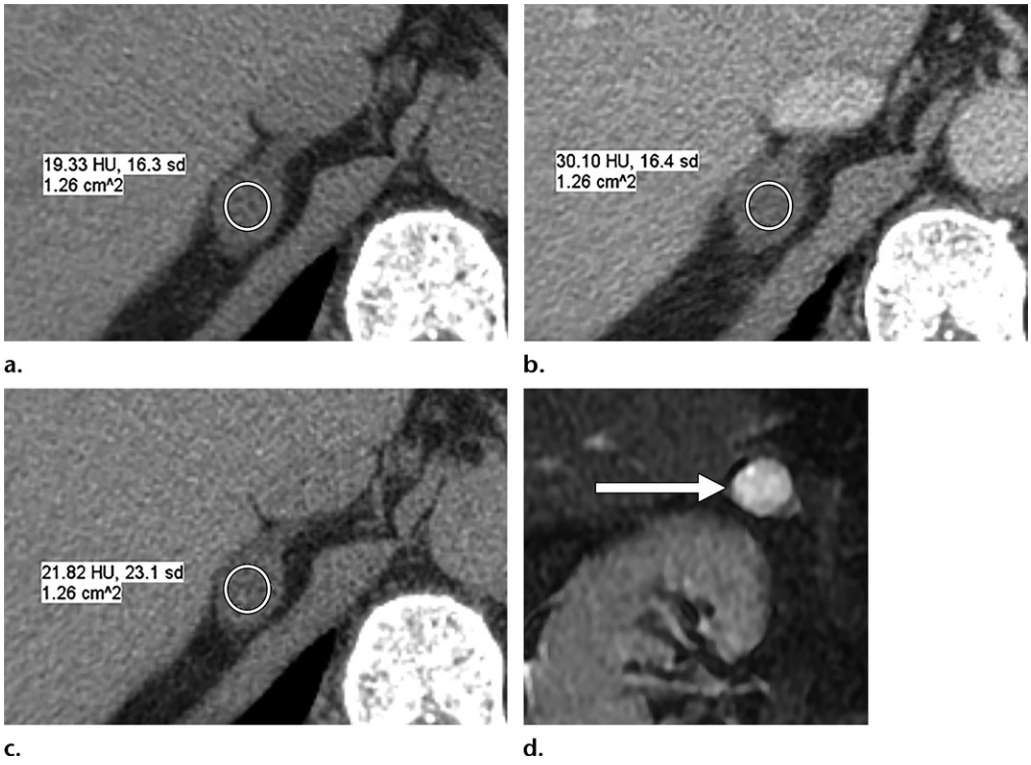

appreciable enhancing component may suggest an underlying lesion (53).

In the context of trauma, evaluation for coexistent associated subtle injuries is useful, as these may be present in as many as 96% of cases. Associated visceral injuries are most frequently seen in the liver (43%) and spleen (23%). Retroperitoneal hematoma may also be present (22%), although active hemorrhagic extravasation is only rarely seen (53).

Clinical Significance of Fat

Although adrenal imaging frequently centers around the detection of microscopic fat, macroscopic or bulk fat can also be seen in adrenal tumors, most commonly in myelolipomas. These lesions may manifest as nodules that are isointense relative to retroperitoneal fat at MRI, but it is important to recognize that these lesions do not lose signal intensity at chemical shift MRI (9). The absence of out-of-phase signal loss in a nodule that is T1 isointense relative to retroperitoneal fat may also conceivably be visualized in a range of other pathologic conditions, such as hemorrhage or proteinaceous fluid within a cyst. Frequency-encoded fat-suppressed MRI sequences or CT may be of use to help confirm the presence of bulk fat (Fig 13).

The identification of fat within a lesion does not uniformly confirm benignity, with macroscopic fat also rarely being identified in adrenocortical carcinoma (54). Similarly, microscopic fat, demonstrated as signal loss at chemical shift MRI, can occasionally be demonstrated in malignant pathologic conditions, such as metastases from hepatocellular carcinoma and clear cell renal cell carcinoma (55). Therefore, fat-containing metastases should be a consideration in patients with these primary tumors.

Microscopic or macroscopic fat may be identified within an adrenal gland demonstrating metastasis if contiguous with an adenoma or myelolipoma, respectively, as a so-called collision tumor (Fig 14) (56). Metastatic collision tumors are generally a diagnostic consideration only in patients with known malignancy. This is based on the observation that isolated incidentally detected adrenal metastases in patients without known malignancy or endocrine disturbance are exceedingly rare (2). Evaluation of prior imaging studies may demonstrate progression in appearances or

a.

b.

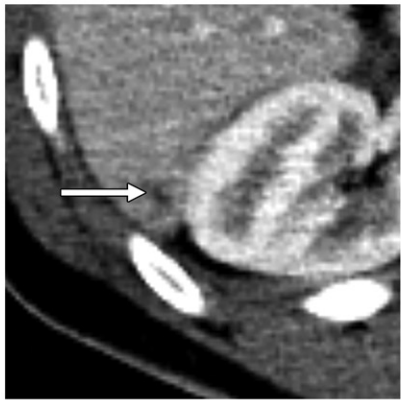

c.

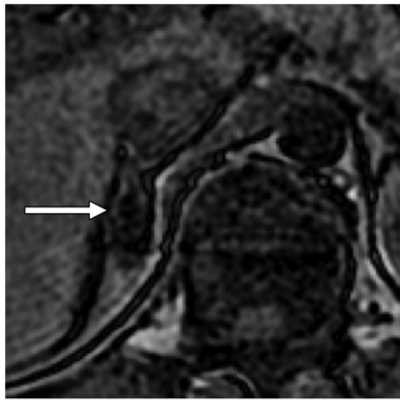

d.

Figure 12. Incidental adrenal pathologic finding at trauma imaging with dual bolus CT. **(a)** Axial CT image shows a right adrenal lesion (arrow) with a 40-HU attenuation value, which was initially considered to be an incidental indeterminate adrenal nodule. In the context of trauma, an apparent incidental adrenal lesion may represent adrenal hemorrhage. **(b–d)** Axial CT images **(b, c)** show, at closer evaluation, haziness of the periadrenal fat (arrow in **b**) and a small associated liver laceration (arrow in **c**). These findings support a diagnosis of adrenal hemorrhage, as does the subsequent resolution (arrow in **d**) on the axial gradient-echo out-of-phase MR image **(d)** obtained at follow-up.

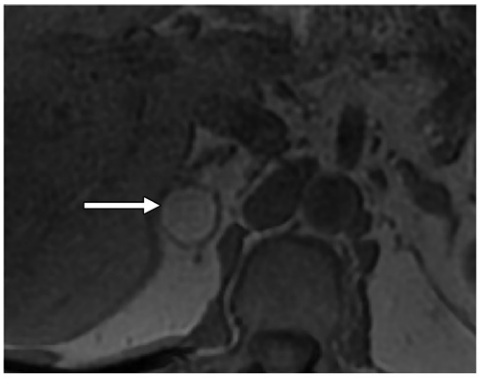

a.

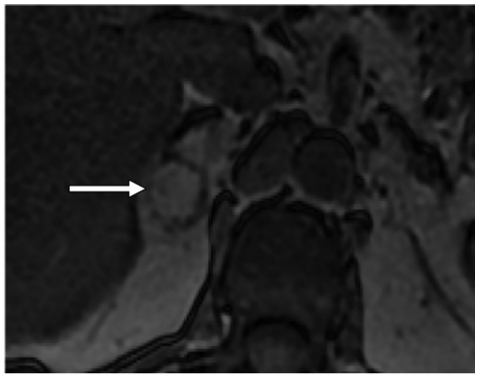

b.

c.

Figure 13. Bulk fat within adrenal lesions. Myelolipomas tend to be isointense relative to retroperitoneal fat at MRI owing to the presence of bulk fat. Unlike microscopic fat, macroscopic fat within myelolipomas does not lose signal. **(a, b)** Axial in-phase **(a)** and out-of-phase **(b)** chemical shift MR images show macroscopic fat within a myelolipoma, which did not lose signal. The absence of out-of-phase signal loss in a nodule that is T1 isointense relative to retroperitoneal fat may also conceivably be visualized in a range of other pathologic conditions, such as hemorrhage or proteinaceous fluid within a cyst. **(c)** Axial nonenhanced CT image shows the presence of bulk fat, consistent with a diagnosis of myelolipoma (arrow).

additional sites of metastases, which would assist in avoiding misdiagnosis. Performing close clinical follow-up, tissue confirmation, or FDG PET/CT may be additive in these circumstances.

Heterogeneity of signal loss and therefore fat content raise the possibility of malignancy including adrenocortical carcinoma and the aforementioned collision tumors. A small proportion of adenomas demonstrate heterogeneous signal loss. However, owing to the greater prevalence of adenomas, a lesion demonstrating signal loss is statistically more likely to reflect an adenoma (57).

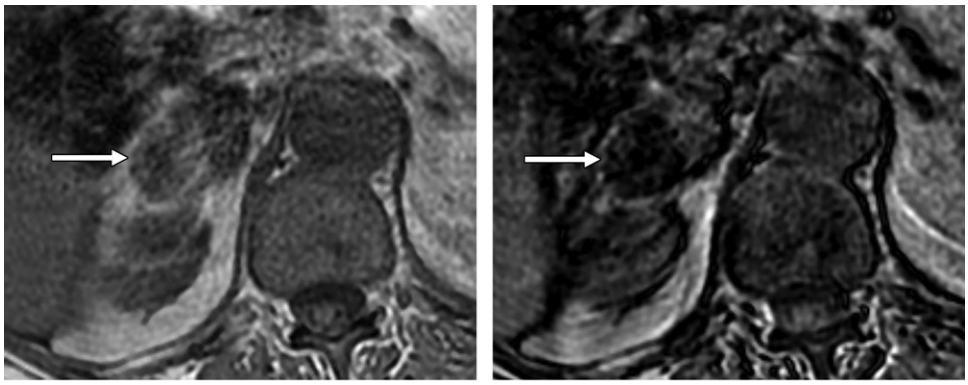

a. b.

Figure 14. Chemical shift MR images in a patient with known lung malignancy, chronic lung disease (accounting for respiratory artifact, depicted here), and known adrenal adenoma show an enlarging heterogeneous right adrenal mass. Axial in-phase **(a)** and out-of-phase **(b)** chemical shift MR images show heterogeneous signal loss. Signal loss is depicted in the lateral component of the lesion (arrow), although no convincing loss is depicted in the medial component, when allowing for signal intensity loss elsewhere in the image. These findings were due to a new metastasis in the medial portion of the gland. The signal loss is within the original adrenal adenoma. The overall imaging appearance reflects a collision tumor, a diagnosis that should be considered in lesions with heterogeneous signal loss, primarily in patients with known malignancy elsewhere.

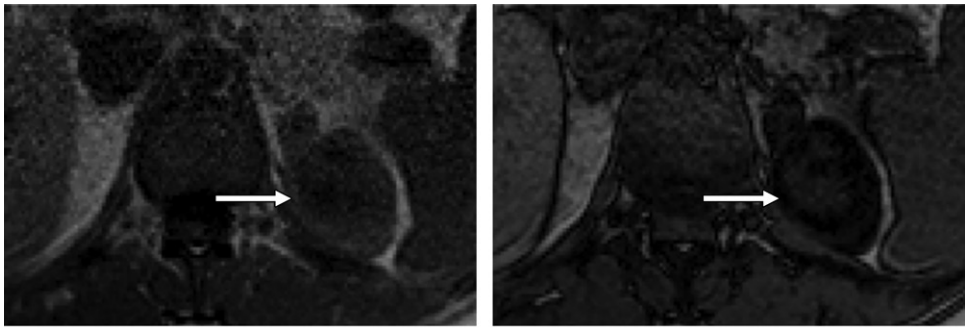

a. b.

Figure 15. Axial in-phase **(a)** and out-of-phase **(b)** chemical shift MR images show heterogeneous signal loss in a histologically confirmed left adrenal adenoma (arrow). Heterogeneous signal loss and therefore fat content raise the possibility of malignancy, including adrenocortical carcinoma and metastatic collision tumor. A proportion of larger adenomas also demonstrate heterogeneous signal loss owing to calcification, cystic change, or myelolipomatous metaplasia.

Heterogeneous signal loss can be visualized in larger adenomas owing to factors such as calcification, cystic change, or myelolipomatous metaplasia (Fig 15) (55).

Clinical Significance of Adrenal Calcification

Adrenal calcification is commonly observed in benign pathologic conditions, typically the sequelae of prior infection or hemorrhage. Calcification is also rarely appreciated in benign adrenal lesions, including cysts, adenomas, and myelolipomas. The presence of calcification does not invariably determine a benign cause, as adrenal calcification may also be identified in malignant pheochromocytomas and in up to 30% of adrenocortical carcinomas (58). The morphology of calcification within adrenocortical carcinoma is variable, with punctate, patchy, or nodular calcification (59). The presence of ancillary features of malignancy, including large size, heterogeneity, and local invasion, is helpful when assessing these lesions (Fig 16) (60).

Atypical Characteristics

Radiologists must be aware of atypical imaging characteristics of common adrenal pathologic conditions to avoid misdiagnosis, such as hemorrhage within adrenal adenomas and focal calcification of myelolipomas (52,60).

Pheochromocytomas are often diagnosed by their typical radiologic features. However, it is important to recognize the pitfall that pheochromocytomas do not always demonstrate such features. This is particularly true with familial paragangliomas such as those that manifest with succinate dehydrogenase mutations (61).

Pheochromocytomas are known to be variable in their appearance, and atypical features

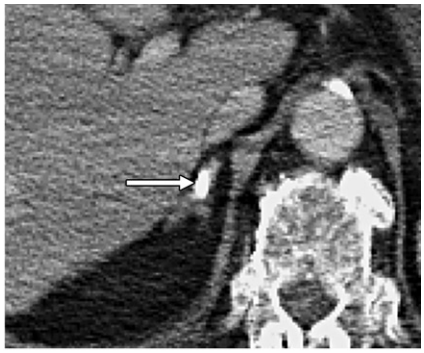

Figure 16. Axial CT images show adrenal calcification. Calcification is commonly identified in benign adrenal pathologic conditions, for example following hemorrhage or infection (arrow in **a**) or rarely in myelolipomas. Arrow in **b** = myelolipoma. It should be remembered that calcification does not consistently confirm benignity and can also manifest in malignant pathologic conditions, including adrenocortical carcinoma (arrow in **c**), as depicted on the nonenhanced CT image **(c)**. Ancillary features of malignancy may help in differentiating it from benign causes, in this case local invasion of the liver and chest wall (arrows in **d**), as depicted on the axial portal venous phase CT image **(d)**.

a.

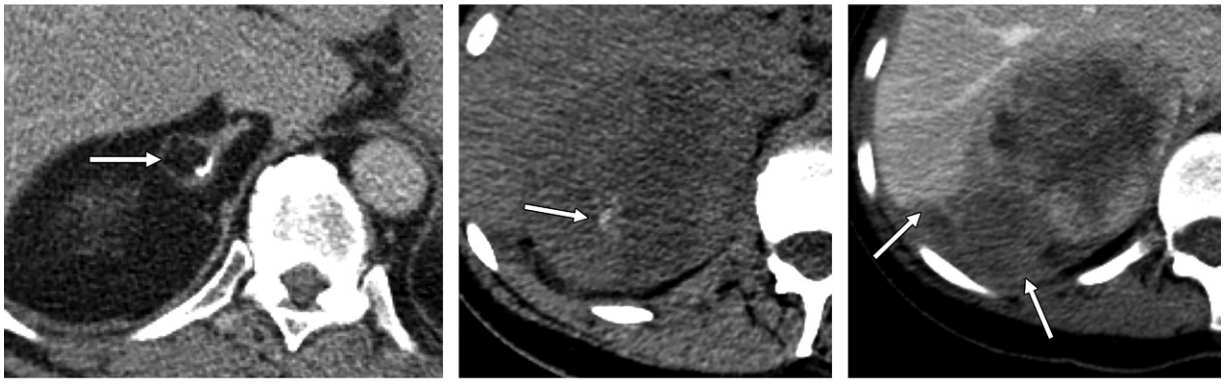

b. **c.** **d.**

Figure 17. Atypical imaging features of pheochromocytoma. The presence of classic imaging features can be helpful for diagnosing pheochromocytomas, although atypical imaging features are often present. Axial portal venous phase CT image **(a)**, MIBG SPECT/CT image **(b)**, and T2-weighted MR image show atypical imaging findings of pheochromocytomas in three different patients with pathologically confirmed right adrenal pheochromocytoma (arrow). These imaging findings include peak enhancement less than 110 HU **(a)**, lack of MIBG uptake **(b)**, and lack of the T2-hyperintense lightbulb sign **(c)**. Histologic and biochemical confirmation are essential in such cases.

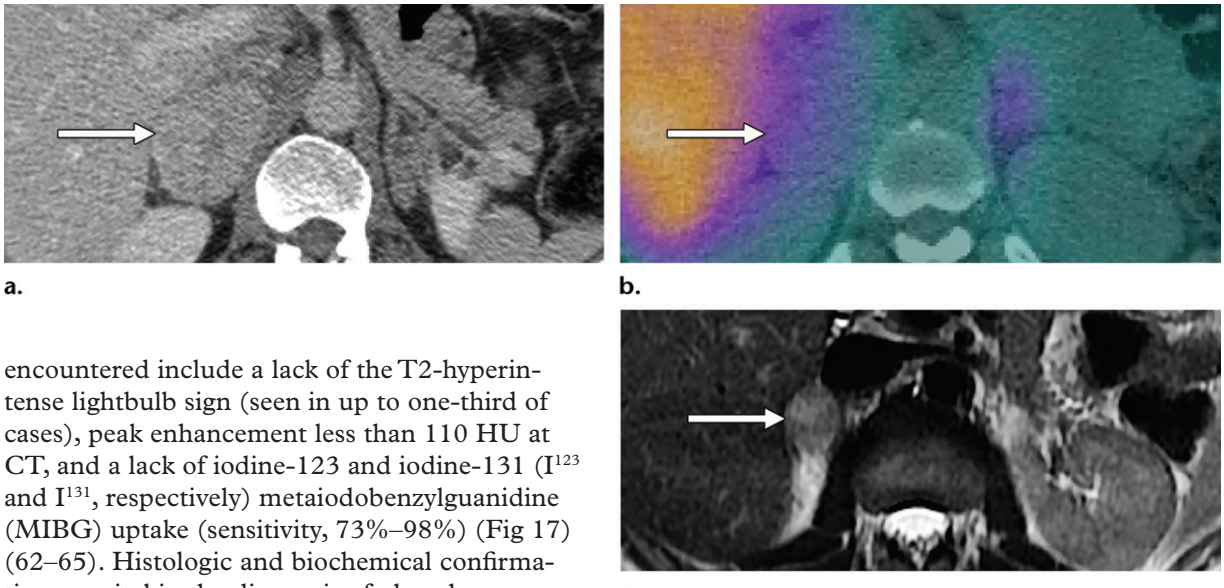

a. **b.** **c.**

encountered include a lack of the T2-hyperintense lightbulb sign (seen in up to one-third of cases), peak enhancement less than 110 HU at CT, and a lack of iodine-123 and iodine-131 (I^{123} and I^{131}, respectively) metaiodobenzylguanidine (MIBG) uptake (sensitivity, 73%–98%) (Fig 17) (62–65). Histologic and biochemical confirmation are vital in the diagnosis of pheochromocytoma, particularly in cases in which there is radiologic uncertainty. Another consideration with pheochromocytomas is that while they can be bilateral, the high prevalence of other incidental pathologic conditions such as adenomas necessitates that an adrenal mass in the contralateral adrenal gland is formally characterized.

Mimics

The anatomy and pathologic conditions arising adjacent to the adrenal gland can simulate adrenal lesions (66). Gastric pathologic conditions can extend into the left suprarenal space

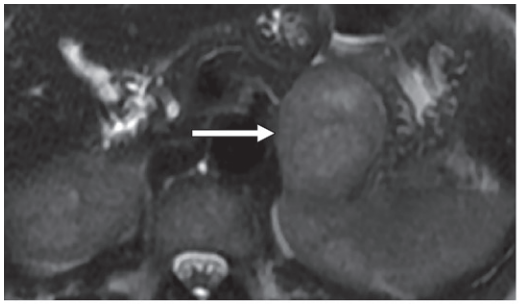

a.

b.

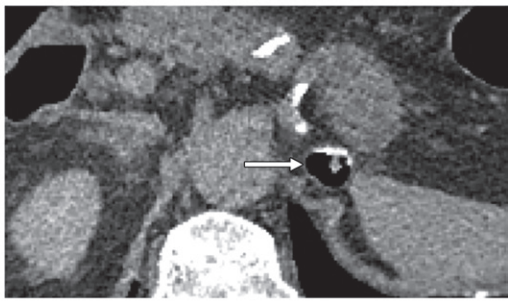

c.

Figure 18. Gastric pathologic conditions may extend into the left suprarenal space and mimic adrenal lesions. **(a)** Axial fat-suppressed FIESTA MR image shows an exophytic gastric gastrointestinal stromal tumor (arrow) with some heterogeneity in signal, a feature found in larger lesions. **(b, c)** Axial CT image in a different patient, obtained with the patient in the supine position **(b)**, shows a suspected gastric diverticulum (arrow in **b**). This was confirmed owing to the presence of gas and mobile oral contrast material within the diverticulum (arrow in **c**) on the image obtained with the patient in the prone position **(c)**.

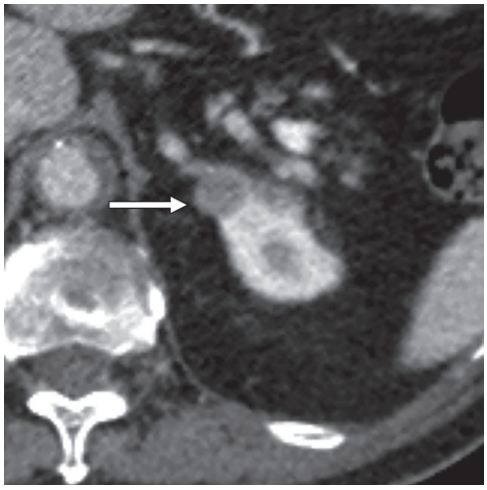

Figure 19. Renal mimics of adrenal pathologic conditions. Axial postcontrast CT image shows a lesion (arrow) contiguous with the left adrenal gland and upper pole of the left kidney. A left renal cyst (attenuation, 11 HU) was diagnosed owing to the presence of the claw sign, which favors a renal origin.

and mimic adrenal lesions. These include gastric diverticula and exophytic gastric tumors, such as gastrointestinal stromal tumors (Fig 18). Pathologic conditions elsewhere in the gastrointestinal tract can also mimic adrenal lesions, including occasionally a fluid-filled colon.

Pathologic conditions arising from the solid viscera can extend into the suprarenal space, with commonly encountered mimics including splenic lobulation, accessory splenic tissue, upper pole renal pathologic conditions, pancreatic tail pathologic conditions, and exophytic hepatic lesions. The presence of the claw sign at imaging may help clarify the organ of origin, particularly with renal pathologic conditions (Fig 19).

Dilated, tortuous, or aneurysmal vessels may resemble adrenal lesions, most commonly splenic varices and splenic artery pseudoaneurysms (Fig 20).

Normal retroperitoneal structures can simulate adrenal pathologic conditions, such as thickened diaphragmatic crura. There are also a variety of retroperitoneal neoplasms that mimic adrenal lesions (Fig 21), including liposarcomas, which can be confused for myelolipomas. A recognized interpretive difficulty with retroperitoneal tumors is that they can distort or invade the adrenal gland, making it difficult to localize the tissue of origin.

Endocrine Function

While CT or MRI cannot consistently help determine endocrine dysfunction, certain radiologic features may manifest that suggest altered endocrine function. If the patient is already known to have endocrine dysfunction, radiologic interpretation should include additional considerations. Potential pitfalls include the failure to identify

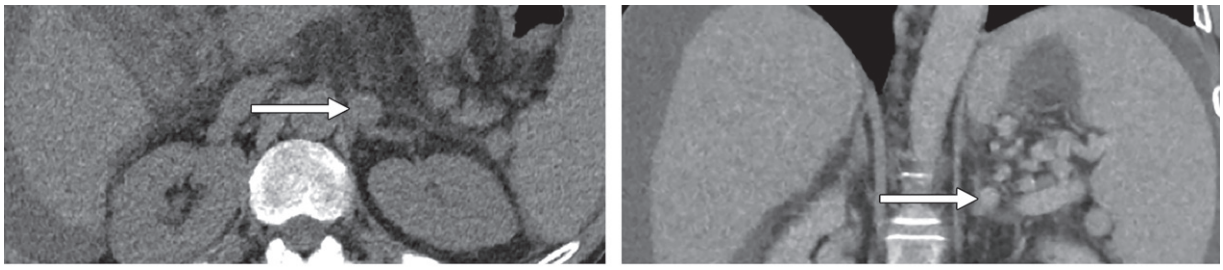

a. b.

Figure 20. Vascular mimics of adrenal pathologic conditions. **(a)** Axial nonenhanced CT image shows a suspected left adrenal nodule (arrow) in a patient with cirrhosis and radiologic features of portal hypertension (splenomegaly, ascites, and varices). Contrast enhancement of the left adrenal nodule follows that of the venous system. **(b)** Coronal portal venous phase reconstructed CT image shows the abnormality to be a splenic varix (arrow). Dilated, tortuous, or aneurysmal vessels may extend into the suprarenal space and mimic adrenal pathologic conditions.

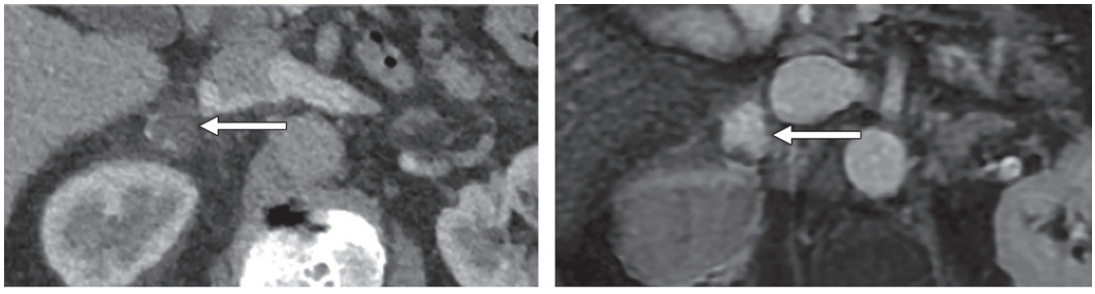

a. b.

Figure 21. Retroperitoneal neoplasms mimicking an adrenal pathologic condition. Axial portal venous phase CT image **(a)** shows a right suprarenal lesion (arrow), with discontinuous peripheral nodular enhancement, which was seen to progressively fill-in, and is hyperintense on the axial fat-saturated FIESTA MR image **(b)**. These findings are consistent with a retroperitoneal hemangioma. A review of multiplanar reformatted images (not shown) showed the lesion arising adjacent to the adrenal gland. Retroperitoneal hemangiomas can also arise from the adrenal gland itself. Imaging characteristics of retroperitoneal hemangiomas can overlap with those of ganglioneuromas, a rare larger adrenal tumor that demonstrates progressive enhancement at postcontrast imaging.

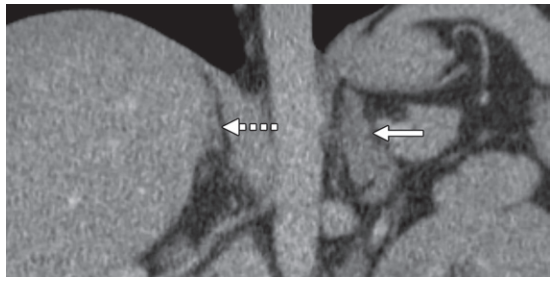

Figure 22. Contralateral adrenal atrophy in a patient with Cushing syndrome. Coronal portal venous phase CT image shows nodular thickening of the left adrenal gland (solid arrow). In this case, the right adrenal gland (dashed arrow) is difficult to appreciate and is atrophic. This is due to endogenous Cushing syndrome with a hyperfunctioning left adrenal gland, which was confirmed by adrenal venous sampling results. The right adrenal gland is atrophic owing to suppression of ACTH.

imaging features that suggest endocrine disturbance, as well as appearances that may determine specific causes or guide appropriate management.

Cushing Syndrome

Adrenocorticotropic hormone (ACTH)–dependent causes comprise the majority of endogenous Cushing syndrome cases (80%) (67). The adrenal glands in such cases are commonly hyperplastic (70%), with mean limb widths greater than 4–5 mm, manifesting as smooth, micronodular, or macronodular hyperplasia. Hyperplasia is more common with ectopic production of ACTH (68). Occasionally, nodular hyperplasia will manifest with a larger nodule and be misinterpreted as an adenoma. Close evaluation for other smaller nodules or limb thickening can help confirm hyperplasia in such cases (69).

The minority of endogenous Cushing syndrome cases are secondary to a primary adrenal cause (20%), with functioning adenomas and less commonly carcinomas being the major diagnostic considerations (67). There may be radiologic signs of a cortisol-secreting tumor, for example contralateral adrenal gland atrophy as a consequence of reduced pituitary ACTH secretion (Fig 22) (69). Furthermore, rarer causes of ACTH-independent Cushing syndrome including primary pigmented nodular adrenal dysplasia (PPNAD)

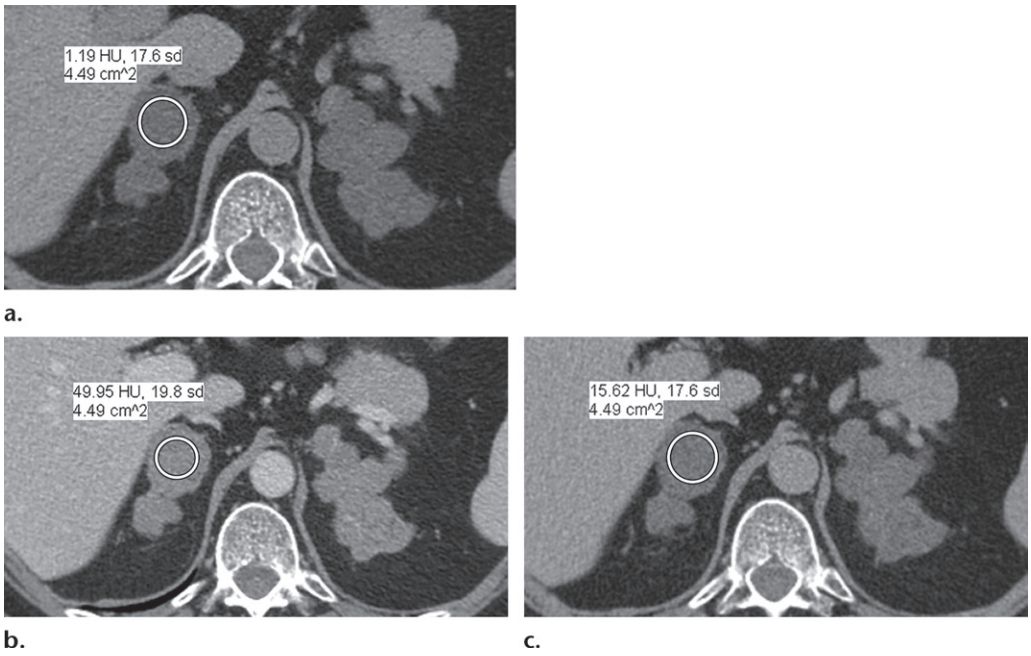

Figure 23. Adrenal gland enlargement in Cushing syndrome. Axial precontrast **(a)**, portal venous phase **(b)**, and 15-minute delayed phase **(c)** CT images show adrenal gland enlargement in a patient with Cushing syndrome. Adrenal gland hyperplasia is found in ACTH-dependent causes of Cushing syndrome. However, the nature of the nodules in this case is not consistent with reactive hyperplasia. Bilateral large (>1 cm) adrenal nodules are depicted, the nonenhanced attenuation of these nodules is less than 10 HU, and the absolute washout is 69% (relative washout, 66%). The attenuation and washout characteristics are consistent with adenoma, but the morphology is suggestive of hyperfunctioning adrenal glands. The diagnosis is, however, not ACTH-dependent Cushing disease but cortisol-producing ACTH-independent macronodular adrenal hyperplasia, characterized by the presence of large nodules (1–5 cm).

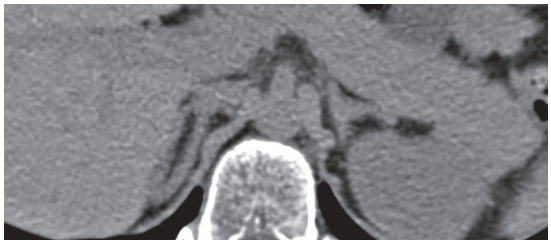

Figure 24. Nonenhanced axial CT image in a patient with histologically confirmed PPNAD shows that the adrenal glands are normal in caliber, which is typical in PPNAD. On occasion, minimal cortical surface irregularity and/or nodularity may be visualized. As the imaging features can be subtle, understanding the clinical context is of utmost importance at diagnosis. In this case, the patient was known to have Carney complex with ACTH-independent Cushing syndrome.

and ACTH-independent macronodular adrenal hyperplasia (AIMAH) have clearly defined radiologic features.

AIMAH is associated with grossly enlarged adrenal glands, with macronodules measuring up to 5 cm and microscopic lipid content (Fig 23). In PPNAD, the adrenals are not significantly enlarged and may appear normal in caliber (Fig 24) but demonstrate multiple small (<5 mm) nodules (these can be 1–2 cm in older patients). Approximately 90%–95% of PPNAD cases occur in patients with Carney complex (70,71).

Conn Syndrome

Primary hyperaldosteronism, due to either aldosterone-producing adenomas (APAs) or bilateral adrenal hyperplasia (BAH), is the most common cause of secondary hypertension. Careful radiologic evaluation is required to differentiate the two, as a solitary-functioning adenoma is usually treated surgically while bilateral hyperplasia is typically treated medically (72). The identification of a nodule must be considered in the context of the remainder of the gland morphology, as the removal of a nodule that is actually part of a diffuse hyperplastic process may be futile (Fig 25). Similarly, the presence of numerous nodules can make the distinction between nodular hyperplasia and adenoma difficult (73).

In such cases, differentiation of APA and BAH in primary hyperaldosteronism may be assisted by measurements of the adrenal limbs, with adrenal hyperplasia associated with enlarged adrenal limbs. The authors of one study conclude that mean adrenal limb measurements greater than 5 mm suggest adrenal hyperplasia (100% specificity) and mean adrenal limb measurements less than 3 mm exclude adrenal hyperplasia (100% sensitivity). With measurements between 3 and 5 mm, it was suggested that performing adrenal venous sampling may be additive to determine the presence of

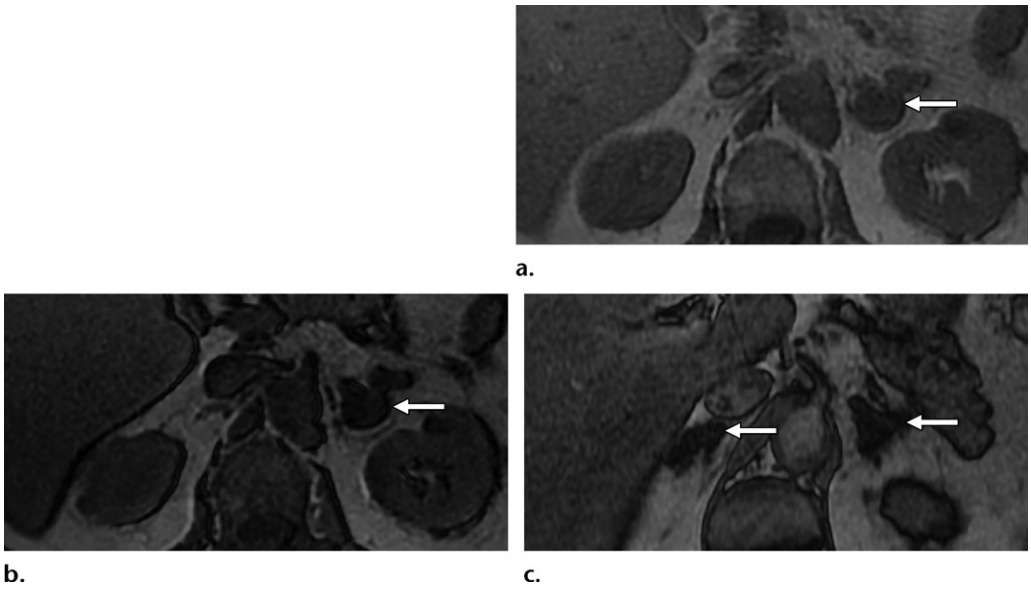

Figure 25. Adrenal hyperplasia versus adrenal adenoma in Conn syndrome. **(a, b)** Axial chemical shift in-phase **(a)** and out-of-phase **(b)** MR images in a patient with hyperaldosteronism show a left adrenal nodule with signal loss (arrow), a finding in keeping with an adenoma, which was presumed to be the cause of primary hyperaldosteronism. Hyperaldosteronism persisted following a left adrenalectomy. **(c)** Axial out-of-phase MR image obtained at initial imaging shows thickening of the left lateral limb and right adrenal gland limbs (arrows). A final diagnosis of bilateral hyperplasia causing hyperaldosteronism was established. This form of Conn syndrome generally requires treatment with medical therapy rather than surgery. Mean adrenal limb measurements (>5 mm, 100% specificity) can aid in differentiating aldosterone-producing adenoma from bilateral adrenal hyperplasia in primary hyperaldosteronism.

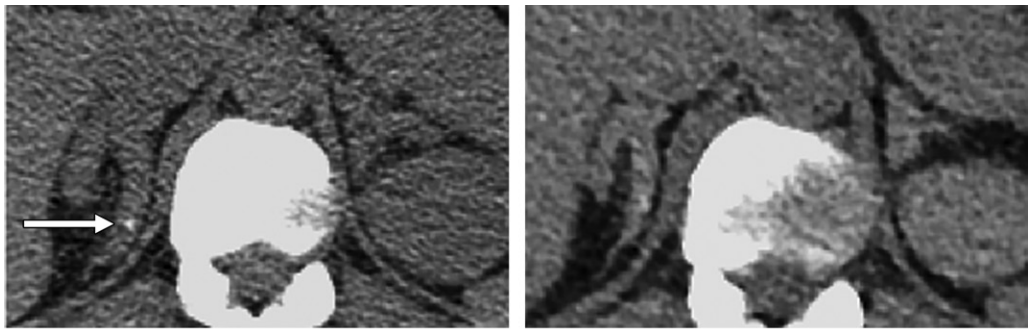

Figure 26. Axial nonenhanced CT image **(a)** in a patient with Addison disease shows bilateral enlargement of the adrenal limbs, which, following a period of tuberculous treatment, reduced in size on the follow-up axial CT image **(b)**. Idiopathic chronic primary hypoaldosteronism may also manifest with adrenal atrophy, but the presence of calcification in this case (arrow in **a**) is indicative of the tuberculous cause.

hyperplasia (74). Ultimately, adrenal vein sampling is important regardless of adrenal limb size, as a proportion of adenomas are small and undetectable, with 20%–50% of aldosterone-secreting adenomas measuring less than 10 mm in size (75).

Primary Adrenal Insufficiency (Addison Disease)

The radiologist usually focuses on identifying focal pathologic conditions of the adrenal gland, which can often be appreciated by a localized increase in the size of the adrenal gland. In contrast, an underlying reduction in the size of the adrenal gland can be subtle and overlooked, particularly as there are no widely used or standardized size criteria to confirm atrophy. A principle cause of adrenal atrophy is Addison disease, although appearances can vary depending on the underlying cause of Addison disease, as well as the phase in the disease course during which imaging has been performed.

For example, granulomatous infection from tuberculosis typically demonstrates bilateral mild to moderate adreniform or masslike enlargement earlier in its disease course. There may be peripheral enhancement with central necrosis at this stage. Adrenal calcification manifests later in the disease process, particularly after treatment when adrenal atrophy may also occur (Fig 26) (76,77). Idiopathic chronic primary hypoaldosteronism

may also manifest with adrenal atrophy, although it typically does not demonstrate calcification (78). Other causes of Addison disease may appear distinctly different radiologically, for example in cases of bilateral adrenal hemorrhage or metastasis.

Conclusion

There are a variety of potential pitfalls when performing and interpreting adrenal imaging. An understanding of the presented technical and interpretive errors, including potential pathologic mimics and features suggesting endocrine disturbance, can improve the accuracy of reporting and may prevent incorrect or inappropriate investigation of adrenal pathologic conditions.

References

1. Bovio S, Cataldi A, Reimondo G, et al. Prevalence of adrenal incidentaloma in a contemporary computerized tomography series. J Endocrinol Invest 2006;29(4):298–302.
2. Song JH, Chaudhry FS, Mayo-Smith WW. The incidental adrenal mass on CT: prevalence of adrenal disease in 1,049 consecutive adrenal masses in patients with no known malignancy. AJR Am J Roentgenol 2008;190(5):1163–1168.
3. Arnold DT, Reed JB, Burt K. Evaluation and management of the incidental adrenal mass. Proc Bayl Univ Med Cent 2003;16(1):7–12.
4. Oliver TW Jr, Bernardino ME, Miller JI, Mansour K, Greene D, Davis WA. Isolated adrenal masses in nonsmall-cell bronchogenic carcinoma. Radiology 1984;153(1):217–218.
5. Korobkin M, Brodeur FJ, Yutzy GG, et al. Differentiation of adrenal adenomas from nonadenomas using CT attenuation values. AJR Am J Roentgenol 1996;166(3):531–536.
6. Lee MJ, Hahn PF, Papanicolaou N, et al. Benign and malignant adrenal masses: CT distinction with attenuation coefficients, size, and observer analysis. Radiology 1991;179(2):415–418.
7. Francis IR, Gross MD, Shapiro B, Korobkin M, Quint LE. Integrated imaging of adrenal disease. Radiology 1992;184(1):1–13.
8. Korobkin M, Giordano TJ, Brodeur FJ, et al. Adrenal adenomas: relationship between histologic lipid and CT and MR findings. Radiology 1996;200(3):743–747.
9. Boland GWL, Blake MA, Hahn PF, Mayo-Smith WW. Incidental adrenal lesions: principles, techniques, and algorithms for imaging characterization. Radiology 2008;249(3):756–775.
10. Caoili EM, Korobkin M, Francis IR, et al. Adrenal masses: characterization with combined unenhanced and delayed enhanced CT. Radiology 2002;222(3):629–633.
11. Boland GWL, Lee MJ, Gazelle GS, Halpern EF, McNicholas MMJ, Mueller PR. Characterization of adrenal masses using unenhanced CT: an analysis of the CT literature. AJR Am J Roentgenol 1998;171(1):201–204.
12. Seo JM, Park BK, Park SY, Kim CK. Characterization of lipid-poor adrenal adenoma: chemical-shift MRI and washout CT. AJR Am J Roentgenol 2014;202(5):1043–1050.
13. Sebro R, Aslam R, Muglia VF, Wang ZJ, Westphalen AC. Low yield of chemical shift MRI for characterization of adrenal lesions with high attenuation density on unenhanced CT. Abdom Imaging 2015;40(2):318–326.
14. Blake MA, Kalra MK, Sweeney AT, et al. Distinguishing benign from malignant adrenal masses: multi-detector row CT protocol with 10-minute delay. Radiology 2006;238(2):578–585.
15. Brooks RA. A quantitative theory of the Hounsfield unit and its application to dual energy scanning. J Comput Assist Tomogr 1977;1(4):487–493.
16. Mayo-Smith WW, Song JH, Boland GL, et al. Management of Incidental Adrenal Masses: A White Paper of the ACR Incidental Findings Committee. J Am Coll Radiol 2017;14(8):1038–1044.
17. Wang B, Gao Z, Zou Q, Li L. Quantitative diagnosis of fatty liver with dual-energy CT. An experimental study in rabbits. Acta Radiol 2003;44(1):92–97.
18. Gupta RT, Ho LM, Marin D, Boll DT, Barnhart HX, Nelson RC. Dual-energy CT for characterization of adrenal nodules: initial experience. AJR Am J Roentgenol 2010;194(6):1479–1483.
19. Shi JW, Dai HZ, Shen L, Xu DF. Dual-energy CT: clinical application in differentiating an adrenal adenoma from a metastasis. Acta Radiol 2014;55(4):505–512.
20. Connolly MJ, McInnes MDF, El-Khodary M, McGrath TA, Schieda N. Diagnostic accuracy of virtual non-contrast enhanced dual-energy CT for diagnosis of adrenal adenoma: A systematic review and meta-analysis. Eur Radiol 2017;27(10):4324–4335.
21. Wortman JR, Sodickson AD. Pearls, Pitfalls, and Problems in Dual-Energy Computed Tomography Imaging of the Body. Radiol Clin North Am 2018;56(4):625–640.
22. Szolar DH, Kammerhuber FH. Adrenal adenomas and nonadenomas: assessment of washout at delayed contrast-enhanced CT. Radiology 1998;207(2):369–375.
23. Park SW, Kim TN, Yoon JH, et al. The washout rate on the delayed CT image as a diagnostic tool for adrenal adenoma verified by pathology: a multicenter study. Int Urol Nephrol 2012;44(5):1397–1402.
24. Sangwaiya MJ, Boland GWL, Cronin CG, Blake MA, Halpern EF, Hahn PF. Incidental adrenal lesions: accuracy of characterization with contrast-enhanced washout multidetector CT—10-minute delayed imaging protocol revisited in a large patient cohort. Radiology 2010;256(2):504–510.
25. Mayo-Smith WW, Lee MJ, McNicholas MM, Hahn PF, Boland GW, Saini S. Characterization of adrenal masses (< 5 cm) by use of chemical shift MR imaging: observer performance versus quantitative measures. AJR Am J Roentgenol 1995;165(1):91–95.
26. Merkle EM, Schindera ST. MR imaging of the adrenal glands: 1.5T versus 3T. Magn Reson Imaging Clin N Am 2007;15(3):365–372, vii.
27. Fujiyoshi F, Nakajo M, Fukukura Y, Tsuchimochi S. Characterization of adrenal tumors by chemical shift fast low-angle shot MR imaging: comparison of four methods of quantitative evaluation. AJR Am J Roentgenol 2003;180(6):1649–1657.
28. Israel GM, Korobkin M, Wang C, Hecht EN, Krinsky GA. Comparison of unenhanced CT and chemical shift MRI in evaluating lipid-rich adrenal adenomas. AJR Am J Roentgenol 2004;183(1):215–219.
29. Outwater EK, Siegelman ES, Huang AB, Birnbaum BA. Adrenal masses: correlation between CT attenuation value and chemical shift ratio at MR imaging with in-phase and opposed-phase sequences. Radiology 1996;200(3):749–752.
30. Bilbey JH, McLoughlin RF, Kurkjian PS, et al. MR imaging of adrenal masses: value of chemical-shift imaging for distinguishing adenomas from other tumors. AJR Am J Roentgenol 1995;164(3):637–642.
31. Yamashita Y, Yamamoto H, Namimoto T, Abe Y, Takahashi M. Phased array breath-hold versus non-breath-hold MR imaging of focal liver lesions: a prospective comparative study. J Magn Reson Imaging 1997;7(2):292–297.
32. Schindera ST, Soher BJ, Delong DM, Dale BM, Merkle EM. Effect of echo time pair selection on quantitative analysis for adrenal tumor characterization with in-phase and opposed-phase MR imaging: initial experience. Radiology 2008;248(1):140–147.
33. Tsushima Y, Dean PB. Characterization of adrenal masses with chemical shift MR imaging: how to select echo times. Radiology 1995;195(1):285–286.
34. Siegelman ES. Adrenal MRI: techniques and clinical applications. J Magn Reson Imaging 2012;36(2):272–285.
35. Northcutt BG, Raman SP, Long C, et al. MDCT of adrenal masses: Can dual-phase enhancement patterns be used to differentiate adenoma and pheochromocytoma? AJR Am J Roentgenol 2013;201(4):834–839.
36. Blake MA, Krishnamoorthy SK, Boland GW, et al. Low-density pheochromocytoma on CT: a mimicker of adrenal adenoma. AJR Am J Roentgenol 2003;181(6):1663–1668.

37. Patel J, Davenport MS, Cohan RH, Caoili EM. Can established CT attenuation and washout criteria for adrenal adenoma accurately exclude pheochromocytoma? AJR Am J Roentgenol 2013;201(1):122–127.
38. Choi YA, Kim CK, Park BK, Kim B. Evaluation of adrenal metastases from renal cell carcinoma and hepatocellular carcinoma: use of delayed contrast-enhanced CT. Radiology 2013;266(2):514–520.
39. Peña CS, Boland GWL, Hahn PF, Lee MJ, Mueller PR. Characterization of indeterminate (lipid-poor) adrenal masses: use of washout characteristics at contrast-enhanced CT. Radiology 2000;217(3):798–802.
40. Blake MA, Holalkere NS, Boland GW. Imaging techniques for adrenal lesion characterization. Radiol Clin North Am 2008;46(1):65–78.
41. Angeli A, Osella G, Alì A, Terzolo M. Adrenal incidentaloma: an overview of clinical and epidemiological data from the National Italian Study Group. Horm Res 1997;47(4-6):279–283.
42. Zeiger MA, Thompson GB, Duh QY, et al. American Association of Clinical Endocrinologists and American Association of Endocrine Surgeons Medical Guidelines for the Management of Adrenal Incidentalomas: executive summary of recommendations. Endocr Pract 2009;15(5):450–453.
43. Mantero F, Terzolo M, Arnaldi G, et al. A survey on adrenal incidentaloma in Italy. J Clin Endocrinol Metab 2000;85(2):637–644.
44. Hanna FWF, Issa BG, Sim J, Keevil B, Fryer AA. Management of incidental adrenal tumours. BMJ 2018;360:j5674.
45. Adam SZ, Nikolaidis P, Horowitz JM, et al. Chemical Shift MR Imaging of the Adrenal Gland: Principles, Pitfalls, and Applications. RadioGraphics 2016;36(2):414–432.
46. Tu W, Verma R, Krishna S, McInnes MDF, Flood TA, Schieda N. Can Adrenal Adenomas Be Differentiated From Adrenal Metastases at Single-Phase Contrast-Enhanced CT? AJR Am J Roentgenol 2018;211(5):1044–1050.
47. Boland GW, Dwamena BA, Jagtiani Sangwaiya M, et al. Characterization of adrenal masses by using FDG PET: a systematic review and meta-analysis of diagnostic test performance. Radiology 2011;259(1):117–126.
48. Tappouni R, Kissane J, Sarwani N, Lehman EB. Pseudoenhancement of renal cysts: influence of lesion size, lesion location, slice thickness, and number of MDCT detectors. AJR Am J Roentgenol 2012;198(1):133–137.
49. Maki DD, Birnbaum BA, Chakraborty DP, Jacobs JE, Carvalho BM, Herman GT. Renal cyst pseudoenhancement: beam-hardening effects on CT numbers. Radiology 1999;213(2):468–472.
50. Kawashima A, Sandler CM, Ernst RD, et al. Imaging of nontraumatic hemorrhage of the adrenal gland. RadioGraphics 1999;19(4):949–963.
51. Jordan E, Poder L, Courtier J, Sai V, Jung A, Coakley FV. Imaging of nontraumatic adrenal hemorrhage. AJR Am J Roentgenol 2012;199(1):W91–W98.
52. Marti JL, Millet J, Sosa JA, Roman SA, Carling T, Udelsman R. Spontaneous adrenal hemorrhage with associated masses: etiology and management in 6 cases and a review of 133 reported cases. World J Surg 2012;36(1):75–82.
53. Sinelnikov AO, Abujudeh HH, Chan D, Novelline RA. CT manifestations of adrenal trauma: experience with 73 cases. Emerg Radiol 2007;13(6):313–318.
54. Egbert N, Elsayes KM, Azar S, Caoili EM. Computed tomography of adrenocortical carcinoma containing macroscopic fat. Cancer Imaging 2010;10(1):198–200.
55. Schieda N, Siegelman ES. Update on CT and MRI of Adrenal Nodules. AJR Am J Roentgenol 2017;208(6):1206–1217.
56. Schwartz LH, Macari M, Huvos AG, Panicek DM. Collision tumors of the adrenal gland: demonstration and characterization at MR imaging. Radiology 1996;201(3):757–760.
57. Gabriel H, Pizzitola V, McComb EN, Wiley E, Miller FH. Adrenal lesions with heterogeneous suppression on chemical shift imaging: clinical implications. J Magn Reson Imaging 2004;19(3):308–316.
58. Dunnick NR, Heaston D, Halvorsen R, Moore AV, Korobkin M. CT appearance of adrenal cortical carcinoma. J Comput Assist Tomogr 1982;6(5):978–982.
59. Zhang HM, Perrier ND, Grubbs EG, et al. CT features and quantification of the characteristics of adrenocortical carcinomas on unenhanced and contrast-enhanced studies. Clin Radiol 2012;67(1):38–46.
60. Hindman N, Israel GM. Adrenal gland and adrenal mass calcification. Eur Radiol 2005;15(6):1163–1167.
61. Cavenagh T, Patel J, Nakhla N, et al. Succinate dehydrogenase mutations: paraganglioma imaging and at-risk population screening. Clin Radiol 2019;74(3):169–177.
62. Varghese JC, Hahn PF, Papanicolaou N, Mayo-Smith WW, Gaa JA, Lee MJ. MR differentiation of phaeochromocytoma from other adrenal lesions based on qualitative analysis of T2 relaxation times. Clin Radiol 1997;52(8):603–606.
63. Lev I, Kelekar G, Waxman A, Yu R. Clinical use and utility of metaiodobenzylguanidine scintigraphy in pheochromocytoma diagnosis. Endocr Pract 2010;16(3):398–407.
64. Van Der Horst-Schrivers ANA, Jager PL, Boezen HM, Schouten JP, Kema IP, Links TP. Iodine-123 metaiodobenzylguanidine scintigraphy in localising phaeochromocytomas--experience and meta-analysis. Anticancer Res 2006;26(2B):1599–1604.
65. Ilias I, Divgi C, Pacak K. Current role of metaiodobenzylguanidine in the diagnosis of pheochromocytoma and medullary thyroid cancer. Semin Nucl Med 2011;41(5):364–368.
66. Gokan T, Ohgiya Y, Nobusawa H, Munechika H. Commonly encountered adrenal pseudotumours on CT. Br J Radiol 2005;78(926):170–174.
67. Lacroix A, Feelders RA, Stratakis CA, Nieman LK. Cushing's syndrome. Lancet 2015;386(9996):913–927.
68. Sohaib SA, Hanson JA, Newell-Price JD, et al. CT appearance of the adrenal glands in adrenocorticotrophic hormone-dependent Cushing's syndrome. AJR Am J Roentgenol 1999;172(4):997–1002.
69. Reznek RH, Armstrong P. The adrenal gland. Clin Endocrinol (Oxf) 1994;40(5):561–576.
70. Rockall AG, Babar SA, Sohaib SAA, et al. CT and MR imaging of the adrenal glands in ACTH-independent cushing syndrome. RadioGraphics 2004;24(2):435–452.
71. Kirschner LS, Taymans SE, Stratakis CA. Characterization of the adrenal gland pathology of Carney complex, and molecular genetics of the disease. Endocr Res 1998;24(3-4):863–864.
72. Patel SM, Lingam RK, Beaconsfield TI, Tran TL, Brown B. Role of radiology in the management of primary aldosteronism. RadioGraphics 2007;27(4):1145–1157.
73. Doppman JL, Gill JRJ Jr, Miller DL, et al. Distinction between hyperaldosteronism due to bilateral hyperplasia and unilateral aldosteronoma: reliability of CT. Radiology 1992;184(3):677–682.
74. Lingam RK, Sohaib SA, Vlahos I, et al. CT of primary hyperaldosteronism (Conn's syndrome): the value of measuring the adrenal gland. AJR Am J Roentgenol 2003;181(3):843–849.
75. Rossi GP, Sacchetto A, Chiesura-Corona M, et al. Identification of the etiology of primary aldosteronism with adrenal vein sampling in patients with equivocal computed tomography and magnetic resonance findings: results in 104 consecutive cases. J Clin Endocrinol Metab 2001;86(3):1083–1090.
76. Ma ES, Yang ZG, Li Y, Guo YK, Deng YP, Zhang XC. Tuberculous Addison's disease: morphological and quantitative evaluation with multidetector-row CT. Eur J Radiol 2007;62(3):352–358.
77. Guo YK, Yang ZG, Li Y, et al. Addison's disease due to adrenal tuberculosis: contrast-enhanced CT features and clinical duration correlation. Eur J Radiol 2007;62(1):126–131.
78. García Pascual L, Simó R, Mesa J, González Atienza J, Vicente de Vera P, Solduga C. Clinical usefulness of adrenal gland computed tomography in the etiologic diagnosis of Addison's disease [in Spanish]. Med Clin (Barc) 1993;101(4):121–124.